CERN-ACC-2018-0047

ruben.garcia.alia@cern.ch

Report

SEU and SEL measurements using 14-MeV and thermal neutron beams

A. Infantino[1], M. Cecchetto[1], R. Garcia Alia[1], M. Marzo[1], M. Brucoli[1], S. Danzeca[1], G. Tsiligiannis[1] , M. Baylac[2], F. Villa[2], J. Segura-Ruiz[3], J. Beaucour[3]

[1]CERN, Geneva, Switzerland
[2]Laboratoire de Physique subatomique et de Cosmologie (LPSC), Grenoble, France
[3]Institut Laue Langevin (ILL), Grenoble, France

Keywords: R2E, Single Event Effect (SEE), LPSC, GENEPI2, ILL, D50

Abstract

A radiation test campaign was carried out at LPSC GENEPI2 (14 MeV neutrons) and ILL D50 (thermal neutron) facilities in order to evaluate the potential use of the beams for Single Event Effect (SEE) characterization of microelectronic components for the Accelerator Technology Sector (ATS) at CERN. Devices that had already been qualified in similar radiation environments were tested as a means of cross-calibration. In this note, the facilities and beam properties are introduced, as well as the comparison results with similar facilities, and an evaluation of the representativeness of 14 MeV for SEEs induced at higher energies (i.e. up to 200 MeV).

Geneva, Switzerland
February, 2018

Contents

1 Introduction

The mixed-radiation field in a high-energy accelerator environment is composed of a broad range of energies and particles [1], with intensities, compositions and spectra that vary significantly throughout the different locations of the accelerator. In particular, shielded areas have radiation fields strongly dominated by neutrons, ranging from thermal to GeV energies. Therefore, qualifying the Single Event Effect (SEE) response of electronic components to such particles in an essential part of the Radiation Hardness Assurance (RHA) strategy in the Radiation to Electronics (R2E) project at CERN.

The test campaign carried out at the LPSC and ILL neutron facilities [2] in February 2017 was first of all focused on evaluating the beam flux, size and homogeneity through dedicated components whose response to similar fields had already been calibrated elsewhere. In addition, tests were performed using the 14 MeV neutron beam at LPSC in order to evaluate its use as a means of screening the SEE response of electronic components to higher energy hadrons. Furthermore, results obtained at LPSC will be compared to those retrieved in the 200 MeV proton beam at PSI, as well as through Monte Carlo simulations.

Moreover, the qualification in the ILL thermal neutron beam had two main objectives. Thermal neutron fluxes in the shielded locations of the LHC accelerator are large, with R-factors (defined as the ration between the thermal and high-energy hadron fluxes) of up to 10-15. Therefore, SRAM based detectors used to monitor the radiation field (such as the RadMON system [3]) need to be accurately calibrated in a thermal neutron field. In addition, in recent years it has been observed that after a decreasing trend in the thermal neutron Single Event Upset (SEU) sensitivity thanks to the removal of boron from the passivation layers (notably BPSG) the relative sensitivity of deep sub-micron CMOS technologies to thermal neutrons has increased [4]. Therefore, an evaluation of the potential impact of such sensitivity on the high-energy accelerator Soft Error Rate (SER) is needed.

This report is structured as follows: Section 2 introduces the LPSC and ILL facilities; Section 3 describes the experimental setups used; Section 4 reports on the flux and homogeneity measurements with calibrated components; Section 5 shows the SEE rests results; and Section 6 completes the report with the summary and conclusions.

2 Facilities description and specific calibration for CERN R2E test campaign

The *Institutes for Research and Technology* (IRT) [2] aims to stimulate the innovation in strategic manufacturing and services industries. Based in Grenoble, France, the IRT Nanoelec is a consortium of 18 partners created in 2012, led by CEA, dedicated to micro/nanoelectronics. Its main objective is to boost research and innovation in microelectronics developed in the renowned global hub of microelectronics located in region. Among the seven IRT Nanoelec programmes, the *Platform of Advanced Characterisation - Grenoble* (PAC-G) aims to provide micro and nanoelectronics access to the powerful characterisation capabilities of Grenoble's large scientific facilities. The PAC-G federates, as core partners for advanced characterisation, the *Institut Laue Langevin* (ILL) [5], the world leading neutron facility operating a very high flux 60MW nuclear reactor, the *European Synchrotron Radiation Facility* (ESRF) and the CEA nano-characterisation resources (CEA/ PFNC: Plateforme de Nano-Characterisation). The *Laboratoire de Physique Subatomique et de Cosmologie* (LPSC) [6] also is part of the PAC-G with its accelerator-based neutron source GENEPI2 used to

study high energy neutron induced Single Event Effects [2]. On the other hand, ST Microelectronics, Soitec and Schneider Electric are the core industrial partners of the platform.

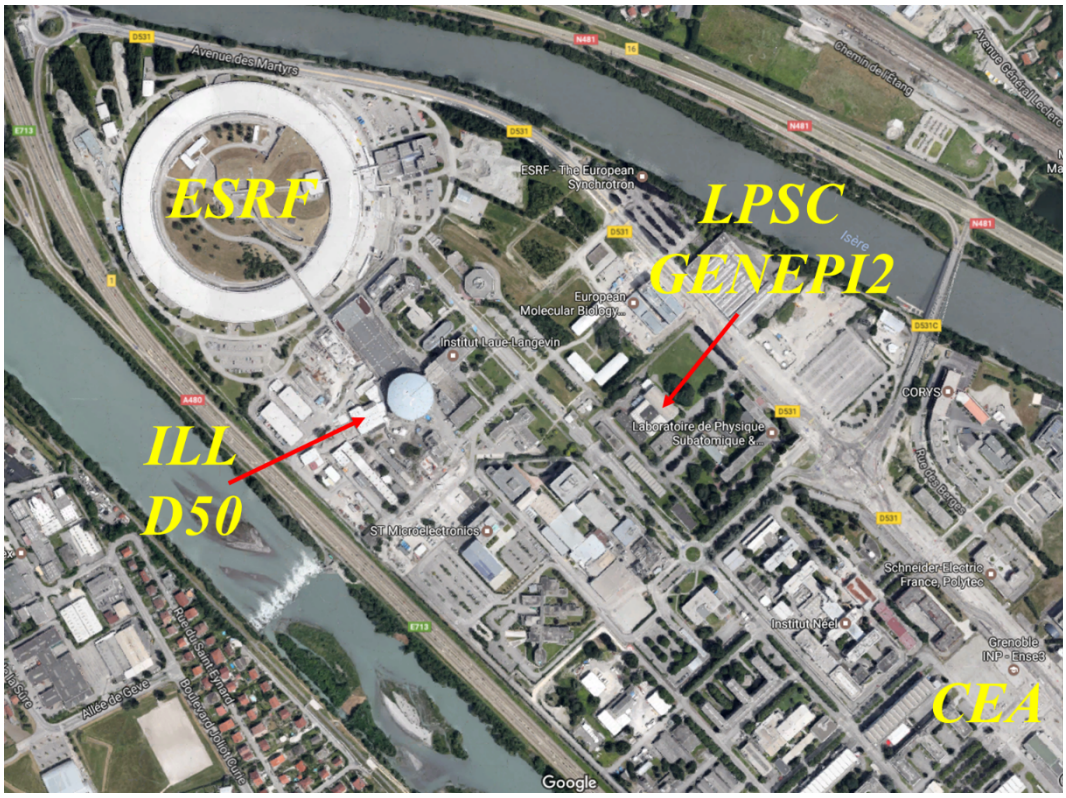

Figure 1 - Overview of the location of the ILL-D50 and LPSC-GENEPI2 facility.

In the following sections, the ILL-D50 and LPSC-GENEPI2 facility (Figure 1) will be presented. After a brief description of the facility, a short summary of the specific calibrations and monitoring for CERN R2E test campaign will be provided.

2.1 LPSC – GENEPI2

2.1.1 GENEPI2: facility description

GENEPI2, *GEnérateur de NEutrons Pulsé Intense* (GEnerator of NEutrons Pulsed and Intense), is an accelerator facility located at LPSC in Grenoble, France. This accelerator was originally developed for nuclear physics experiments. Since 2013, this facility has also been used to irradiate integrated circuits from different technologies [7]. Indeed, the effects of neutrons on electronics, due to their interaction with the nuclei of the device materials, is very well known and documented in the scientific literature, e.g. [8, 9, 10]. On the other hand, the number of facilities able to deliver monoenergetic ±10% (or quasi-monoenergetic) neutron beams, with appropriate energy and flux specifications, is limited. Among these facilities, GENEPI2 has acquired, in recent years, an important role for testing electronics using neutron beams.

GENEPI2 is an electrostatic accelerator able to produce neutrons through the interaction of an accelerator deuteron beam (d) onto a fixed target made of tritium (T) or deuterium (D), depending on the required neutron energy. Neutrons are thus generated by one of the following fusion reactions:

$$d + T \rightarrow {}^{4}He + n \; (\langle E_n \rangle = 14.2 \; MeV)$$
$$d + D \rightarrow {}^{3}He + n \; (\langle E_n \rangle = 2.5 \; MeV)$$

Neutrons are produced through the d-T or d-D process with an average neutron energy of 14.2 MeV or 2.5 MeV respectively [11].

Originally, GENEPI2 (Figure 2) was built for nuclear cross-section measurements supporting future nuclear reactor concepts: this field required neutrons to be produced within short bunches such that they can be tagged with a time reference. To generate the deuteron beam, a duoplasmatron source was used as it can provide the appropriate time structure by pulsing the ionizing plasma. Thus ions were produced in the form of short and intense bunches (FWHM < 1 μs, peak ~50 mA). Beam bunches were produced with a repetition rate which can be adjusted between 10 Hz and 4.5 kHz. The average deuteron intensity, and therefore the neutron production rate, was adjusted by changing the beam repetition rate.

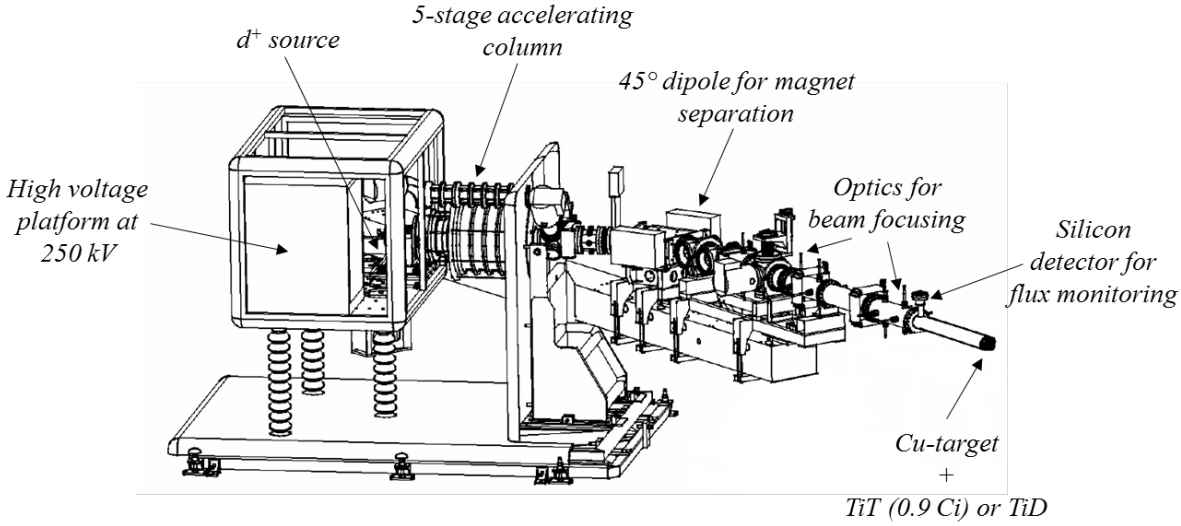

Figure 2 - Layout of the GENEPI2 accelerator providing neutron beams of the order of 2.5-MeV or 14-MeV [11]. The main component of the GENEPI2 accelerator are indicated in the picture and described in details in the text.

In 2017, the facility had a major upgrade concerning the ion source: an Electron Cyclotron Resonance (ECR) source was installed, replacing the duoplasmatron source. Ion sources of ECR type produce an intense and continuous beam [12], thus generating an enhanced neutron flux and purely continuous. The flux remains easily adjustable by tuning the ion source beam current and it is foreseen to reach a neutron rate of 1.0E+10 s^{-1} for the d-T reaction [11]. The ion source sits within a high voltage platform held at a constant voltage of 250 kV with respect to ground, itself surrounded by a Faraday cage. The ions are extracted and focused by a series of 5 conical high voltage electrodes, shaping the deuteron beam. This beam is accelerated up to 250 keV by a 5-stage accelerating structure. After acceleration, beam is transported through a 5 m long beam line, held under vacuum (~10^{-7} mbar) to minimize interactions with residual gas. The deuteron beam is bent by a 45° electromagnet performing a magnetic selection: deuterons are consequently transported towards the target while other species, which can be produced by the source in a small fraction, are dumped on a dedicated ion collector. High intensity handling is achieved with constant focusing along the beam line every ~0.5 m by a series of electrostatic quadrupoles with cylindrical electrodes. Beam diagnostics are placed at different locations to characterize the beam intensity and profile. Magnetic steerers allow fine beam position adjustment on the target. The beam dimensions are tuned to match the active area of the target (25 mm in diameter), which is placed at the end of the beam line. The beam intensity is measured on target continuously. The target active area is made of a titanium layer loaded with tritium (TiT) or deuterium (TiD) deposited on a high purity copper disk. The activity of a fresh tritium ($T_{1/2}$ =

12.33 years) target is 0.9 Ci[1]. This initial activity decreases with beam operation because of tritium release caused by beam impact and target heating. Consequently, the target is air-cooled to limit tritium (or deuterium) desorption. Temperature is permanently controlled at the back side of the target. Typically, a target can be used for 6 months/1 year before depletion in the present operational conditions of GENEPI2.

Neutrons are emitted from the target and the device under test (DUT) is placed directly facing it. The entire facility is shielded by a concrete bunker. The accelerator is entirely controlled and operated remotely via a command control system [11]. In early 2017, a fresh tritium target was installed, generating a maximum neutron flux of 4.5E+07 $cm^{-2}s^{-1}$ at distance of 34 mm from the target plane. Under these conditions, DUTs are exposed, within one hour, to a fluence of 1.6E+11 cm^{-2} of 14.2 MeV neutrons [2].

2.1.2 Neutron flux monitoring and characterization at GENEPI2

Due to the physics of the fusion reactions, the neutron flux has an angular distribution: indeed, the neutron energy depends on the emission angle. For an incident beam energy of 250 keV, the d-T cross section is nearly isotropic such that neutrons spread evenly in all directions from the target. The neutron energy, slightly depending on the emission angle θ between the neutron direction and the beam axis, averages to 14.2 MeV for d-T and 2.5 MeV for d-D processes. The neutrons emitted fully forward (θ ~ 0°) carry the maximum energy, namely ~15 MeV with a tritium target (Figure 3) or 3 MeV for a deuterium target [11].

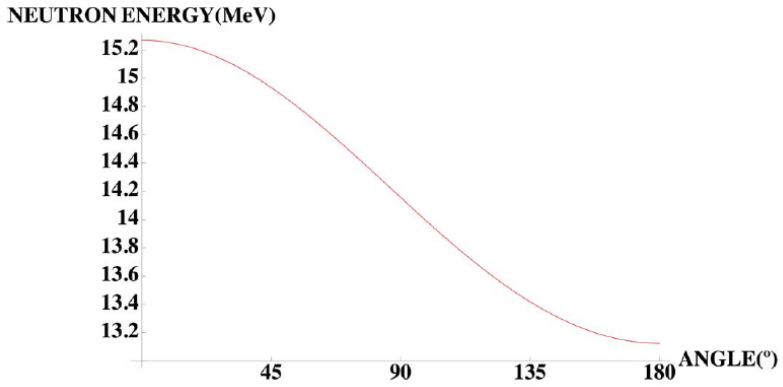

Figure 3 - Theoretical energy of neutrons produced via d-T reactions as a function of the angle between the neutron direction and the beam axis for an incident beam energy of 250 keV [11].

The neutron flux produced by GENEPI2 is assessed and monitored through different systems. The neutron flux can be preliminary monitored through the real-time monitoring of the deuteron beam current impinging on the target: indeed, the neutron flux is proportional to the deuteron beam current. The beam current is logged into a log file every second, thus providing relative variations of the neutron flux. The current stability is typically within ± 3% rms (root mean square). To obtain the absolute calibration of the neutron flux, the activation technique was used. ^{27}Al foils (purity 99,99%) were exposed to a 14 MeV neutron flux at a reference position of 34 mm from the target surface, with a reference current. The measurement of the induced activity was performed at the *Low Activity Laboratory* (LBA) [13] of the LPSC using a Germanium detector. The neutron flux measurement was based on the decay of ^{27}Mg ($T_{1/2}$ = 9.458 min) and ^{24}Na ($T_{1/2}$ = 14.958 hours), induced in the foils by the following two reactions:

[1] 1 Ci = 37E+09 Bq

$$n + {}^{27}Al \rightarrow {}^{27}Mg + p$$
$$n + {}^{27}Al \rightarrow {}^{24}Na + \alpha$$

The neutron flux, expressed in $cm^{-2}s^{-1}$, is then calculated through inverting the activation equation:

$$\dot{\phi} = \frac{A}{N_0 \sigma (1 - e^{-\lambda t})}$$

where A is the activity in Bq (corrected by the transportation time and the measurement time), N_0 is the total number of target atoms (^{27}Al) in the foils taking into account the isotopic abundance, t is the irradiation time, λ is the decay constant of ^{27}Mg or ^{24}Na (i.e. $\ln(2)/T_{1/2}$) and finally σ is the reaction cross section, in cm^2 (Figure 4). For 14 MeV neutron $\sigma_{^{27}Al(n,p)^{27}Mg}$=0.07 barn and $\sigma_{^{27}Al(n,\alpha)^{24}Na}$=0.12 barn.

The regular monitoring of the neutron flux, with such activation measurements, allows to assess the target aging: indeed, the total amount of Tritium available in the target reduces as the facility is operated over several months. As a consequence, a decreasing number of fusion reactions takes place, translating in a reduced neutron flux. Therefore, it is possible to monitor, by repeating the activation measurements over time, the neutron production for a given beam intensity, as a function of the cumulated charge on the target. Typically, within a year of regular operation of the facility, The neutron production drops as the charge, deposited by the beam, is accumulated on the target. The neutron flux is maintained at the required level by increasing the beam current to compensate the target ageing. Along the year, the neutron flux is maintained at the level required for users by increasing the beam current to compensate the target ageing.

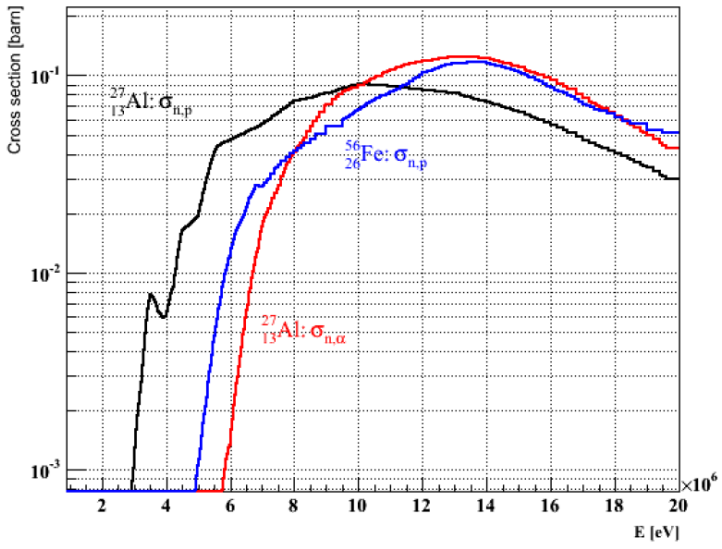

Figure 4 - Cross sections for different neutron activation processes as a function of the neutron energy. Activation measurement of GENEPI2 flux, internal report.

In addition, the neutron flux can be directly monitored by silicon detectors which can be used for both 3 MeV and 15 MeV production. The monitoring is based on the detection of particles associated to the neutron production. The semiconductor detectors sit under vacuum within the beam line, approximately 0.6 m upstream the target (Figure 5).

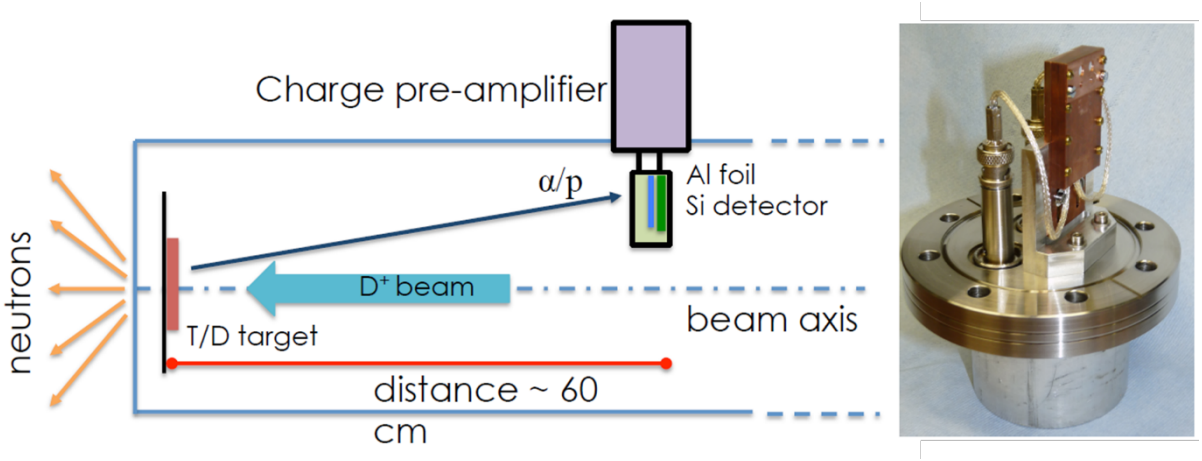

Figure 5 - Silicon detector used for direct flux monitoring.

The detection is performed under direct solid angle from the target in order to collect particles which are scattered backwards. When operating with the tritium target, the detector collects α particles emitted from the target from the T(d,n)α reaction. The recorded energy spectrum is analysed off line to determine the total number of collected α particles per unit time, $N_{\alpha_{detected}}$, taking into account event multiplicity. The absolute number N_n of 15 MeV neutrons emitted in full space per unit time is provided by the total number of emitted α particles, N_n. Given the solid angle covered by the detector ($\Delta\Omega$), N_n is determined by [11]:

$$N_n = N_\alpha = N_{\alpha-detected} \times \frac{4\pi}{\Delta\Omega}$$

Similarly, the detector can provide the absolute monitoring of 3 MeV neutrons. When bombarding a deuterium target with a deuteron beam, two reactions take place:

$$d + D \rightarrow {}^3He + n$$

$$d + D \rightarrow T + p$$

The second process is used to monitor the 3 MeV neutron production, as the detector collects the emitted protons. The absolute number of 3 MeV neutrons emitted in full space per unit time is thus determined based on the proton counts, instead of α particles. A correction factor must be applied as the two d-D reactions are not exactly equally probable.

The neutron flux in $cm^{-2}s^{-1}$ at any location can be calculated by scaling the total number of neutrons per unit time N_n at a distance r from the target [11]:

$$N_n(r) = \frac{N_n}{4\pi r^2}$$

Finally, an additional monitor can be used to characterize the emission of neutrons from the T(d,n)α reaction. The 15 MeV neutrons are converted into recoil protons via a (n,p) reaction on a layer of Polyethylene. Protons are then detected through a 3-stage Si telescope with a triple coincidence. In order to reach the last stage of silicon, protons must have a minimum energy of about 9 MeV downstream of the converter. The intrinsic detection efficiency of the monitor is ~0.1% [14, 6]. This detector sits outside vacuum, it is disconnected from the beamline and can be placed wherever needed in the experimental room.

From the combination of the different methods, it is possible to get a precision better than ±15% on the flux measurement in the 1-15 MeV energy range.

To cross-validate the facility, radiation tests on a 90-nm CYPRESS CMOS SRAM memory were performed with 15 MeV neutrons. This device was chosen because it was previously tested in other radiation facilities, including ASP [15], TRIUMF [16] and KVI [17]. The SRAM was mounted facing the centre of the target, perpendicularly to the beam axis, at an distance adjustable depending on the desired neutron flux. The results (Figure 6) found at GENEPI2 are compatible with one obtained at ASP [6]. Tests on integrated circuits contribute to the characterization of GENEPI2, as shown in Figure 7: the comparison between the neutron flux measurements performed through activation foils and SEUs, generated in a highly sensitive low power SRAM, is reported and can be used as flux reference [6].

Finally, the flux homogeneity was studied. It was first measured as the accelerator was driven by the pulsed duoplasmatron source through a board provided of a matrix of 75 SRAM 4-Mbit CY7C1041D memories (GoldenBoard EASii-IC). Measurements were conducted at a distance of 1 and 3 cm from the target respectively. The results of the flux homogeneity are reported in Figure 8. Recently, it has been assessed with neutrons produced with the ECR ion source installed in 2017. Preliminary results show that the homogeneity is maintained with this ion source.

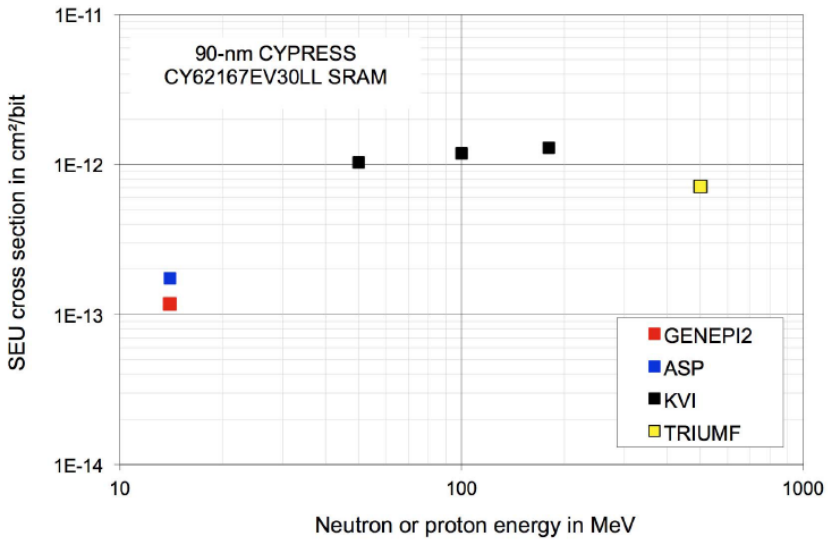

Figure 6 – Comparison of the SEU measurement of a 90-nm CYPRESS CMOS SRAM memory performed at GENEPI2 and other reference facilities [6].

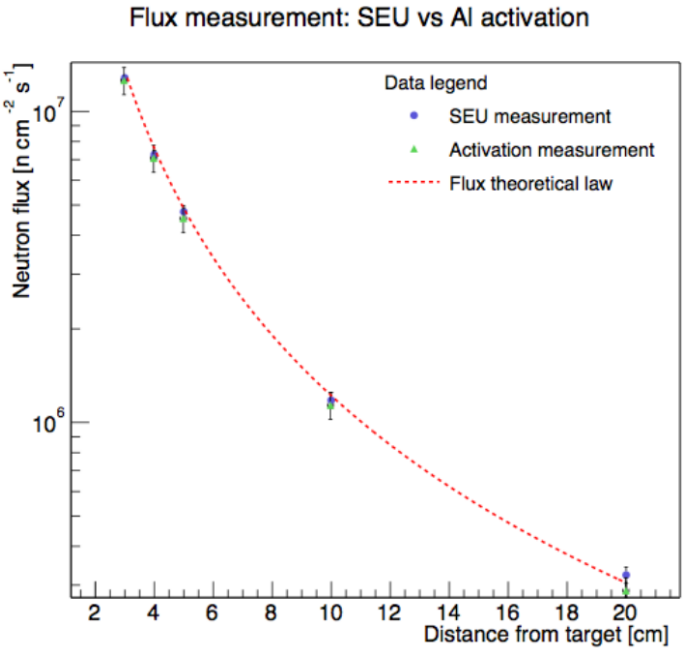

Figure 7 – Characterization of the GENEPI2 facility: comparison between activation and SEU measurements at different distances from the target. The results agree better than 4% [6].

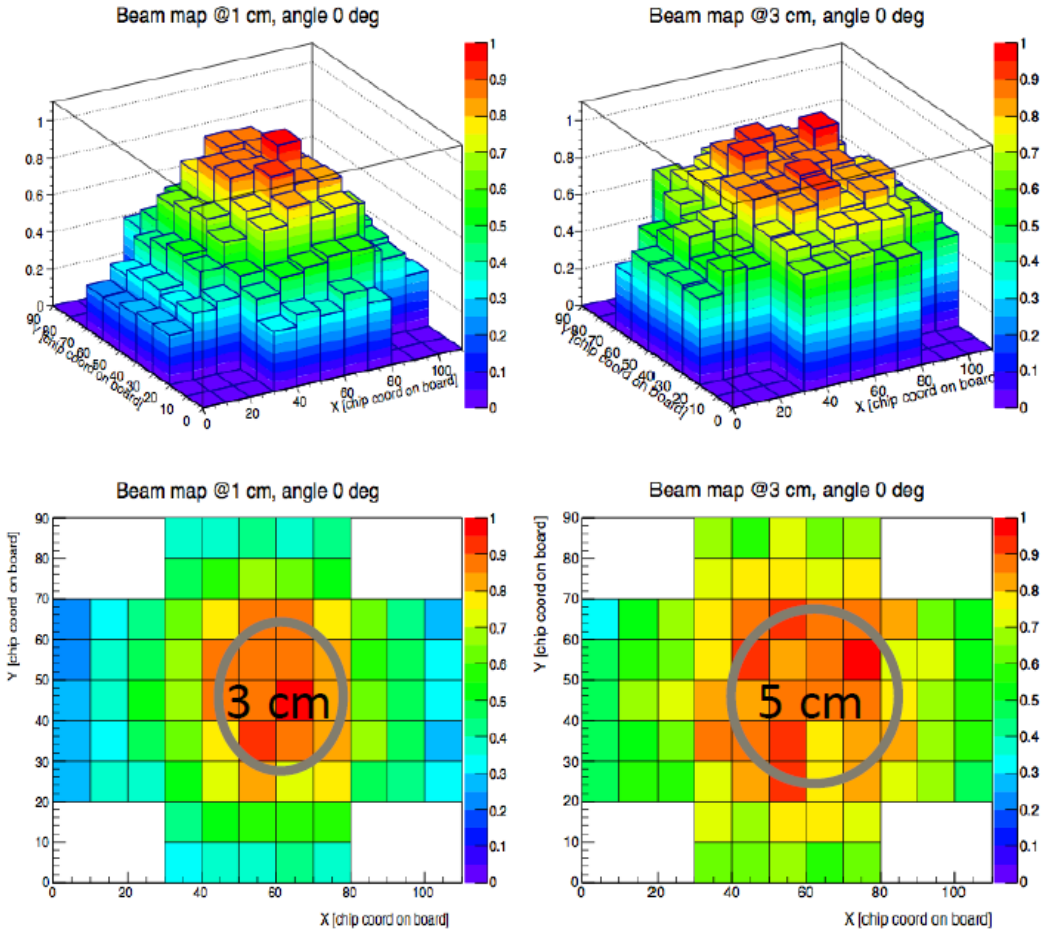

Figure 8 - Flux homogeneity assessment at GENEPI2 using the previous duoplasmatron source: the neutron flux resulted homogenous (+/- 10%) within an area of 3 cm and 5 cm, in diameter, at a distance of 1 cm and 3 cm from the target respectively. Y axes represent the relative intensity.

In conjunction with CERN's February 2017 test campaign, two activation measurements have been performed to assess the neutron flux (Table 1). The neutron flux has been assessed at the reference distance of 34 mm from the target, which will be used as reference distance in the following of the report. Measurements have been performed before and after CERN test campaign. The neutron flux is reported, by convention, at the reference beam current of 150 μA. At the time of the CERN test campaign, the facility provided a reference neutron flux, used in the following data analysis, of 3.20E+07 $cm^{-2}s^{-1}$ at 34 mm and 120 μA.

Table 1 - Neutron flux assessment at GENEPI2 through activation measurements: the difference between the two measurements is attributed to the target ageing.

Date	***Distance target-foil [mm]***	***Average Current [μA]***	***Neutron Flux [$cm^{-2}s^{-1}$]***	***Flux @ 150 μA [$cm^{-2}s^{-1}$]***
20 January 2017	34	117	(3.22 ± 0.13)E+07	4.13E+07
14 February 2017	34	157	(4.09 ± 0.12)E+07	3.91E+07

2.2 ILL – D50

2.2.1 ILL and the D50 instrument: facility description

The "*Institut Laue Langevin*" **[5]** and the High Flux Reactor are located north of the Grenoble scientific area (Figure 1) and is managed by three associated countries, France (CEA and CNRS), Germany and UK, in association with several Scientific Member countries. The ILL High Flux Reactor operates continuously during 50-day cycles. Its heart is consisting of a single fuel element of highly enriched Uranium 235, cooled and moderated with heavy water (D_2O), to produce the most intense neutron flux in the world, namely 1.5E+15 $cm^{-2}s^{-1}$. A total thermal power of 58 MW is generated: this power is dissipated by a secondary power circuit. The heavy water tank containing the fuel element is located in a pool filled with water which provides protection against neutron and gamma radiation emitted by the reactor core. The reactor is driven by means of 5 control bars which is able to absorb neutrons. The reactor is provided with other additional 5 safety bars, whose function is the emergency shutdown **[5]**.

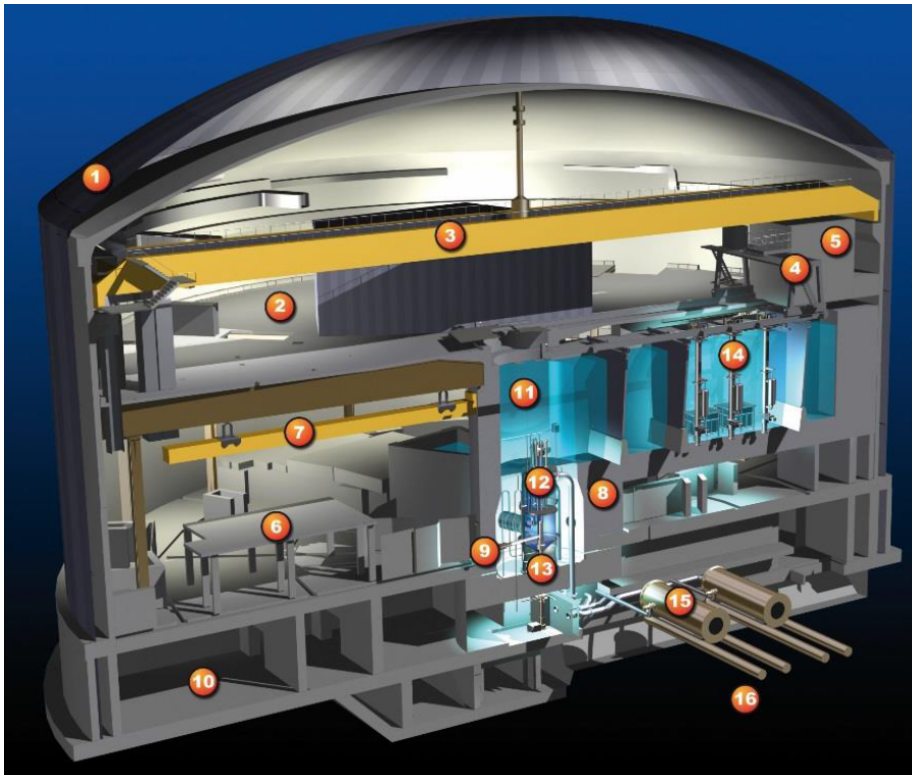

Figure 9 – Section of the ILL reactor building. 1) Double container of the reactor building, 2) Level D – Operation Hall, 3) Crane Level D, 4) Crane gantry, 5) Hot cell, 6) Level C – Experimental Hall, 7) Crane Level C, 8) Biological protection, 9) Extraction line of collimated neutron beam, 10), Level B – Auxiliary Equipment, 11) Reactor Pool (light water), 12) Primary circuit (Heavy water – cooling and moderation), 13) Fuel element, 14) Spent fuel storage, 15) Primary to secondary circuit heat exchanger, 16) Secondary cooling circuit [5].

Neutrons are produced in the reactor from the fission reactions of the Uranium nuclei: prompt neutrons have a very high energy corresponding ~20,000 km/s **[5]**. They are slowed down to thermal energy (0.025 eV, ~2.2 km/s) by the heavy water in order to be able to produce new fissions and to maintain the reaction chain self-consistent as well as to provide thermal neutrons beams to all the experiments. Three devices, located in the immediate vicinity of the reactor core, make it also possible to produce "hot" (10 km/s), cold and ultra-cold (700 m/s and 10 m/s) neutrons. The hot source consists of a sphere of graphite maintained at 2600 °C; two cold sources are also available, the largest of which

consists of a sphere containing 20 litres of Deuterium maintained in liquid phase at -248 °C and in which neutrons are slowed down to the desired energy by a succession of collisions with the Deuterium nuclei. The neutrons are then extracted from the tank through 20 channels, some of which point to one of the cold or hot source. These channels, extended by neutron guides, provides neutron beam over more than 40 experimental areas (Figure 10) **[5]**. One of these areas is the D50 instrument where the tests have been performed, which will be explained in details in the following.

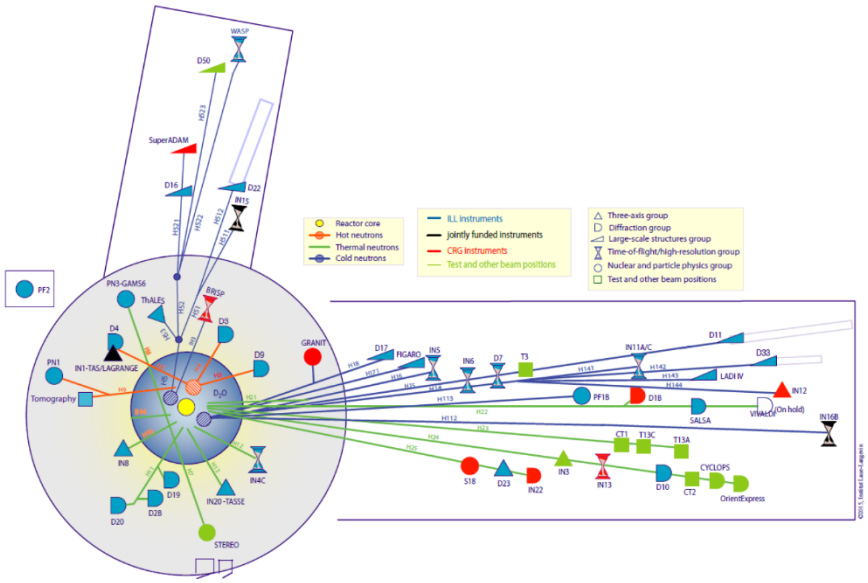

Figure 10 - Experimental areas available at ILL [5].

Neutrons allow to explore matter in a non-destructive way. They are actually used in many scientific fields such as physics, chemistry, biology and biotechnology, nanotechnology, geosciences or engineering civil. The principle of the majority of experiments is always the same: scientists place the sample of a material to be studied in the neutron beam; the detection and measurement of scattered neutrons provides them information on the physical characteristics of their sample **[5]**.

2.2.2 The D50 instrument

D50 (Figure 11) is a scientific instrument fully dedicated to industrial activity, including but not restricted to microelectronics. It makes accessible the neutron techniques mostly demanded by the microelectronics industry: neutron reflectivity, cold neutrons irradiation and neutron tomography with resolution in the range of a few microns.

Figure 11 - The D50 instrument at ILL (Courtesy of J. Segura-Ruiz).

The technical specification of the cold neutron irradiation facility available on D50 has been defined in collaboration with industrial partners. The neutrons available on D50 are produced by the ILL horizontal cold source (thermal neutrons moderated by liquid deuterium at 20°K) and transmitted along a 100 m long neutron-guide. The captured flux (i.e. equivalent flux of 25 meV neutron) delivered on D50 is adjustable from 0 to 1.0E+10 $cm^{-2}s^{-1}$, with optimisation for flux range from 1.0E+06 to 1.0E+08 $cm^{-2}s^{-1}$. The neutron spot size may be easily adapted for local irradiation (1 mm^2) to global irradiation of homogeneous square section of about 5000 mm^2 by means of motorised borated carbon (B_4C) slits. The neutron flux is controlled with dedicated scintillator-based neutron detector and periodical gold foil measurements to achieve reliable flux data. A sample changer makes possible successive irradiations of components and boards (150 x 170 mm). The typical neutron spectrum available at D50 is reported in Figure 12.

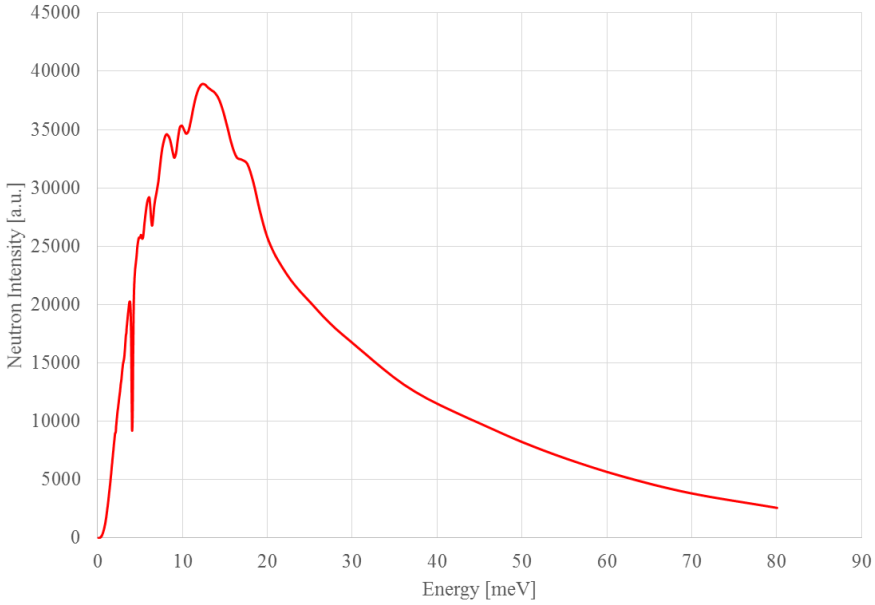

Figure 12 - ILL-D50 neutron spectrum (Courtesy of J. Segura-Ruiz) [18].

2.2.3 Neutron flux monitoring and characterization at D50

The neutron flux is periodically assessed by the activation of Gold foils, similarly to what already reported for GENEPI2 in section 2.1.2. Five Gold foils of a diameter of 10 mm are placed on the beam as shown in Figure 13.

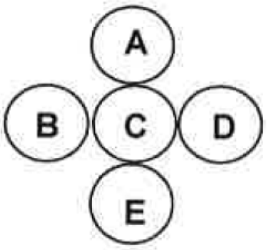

Figure 13 – Principle of flux and beam profile measurements at ILL-D50 by activation of Gold foils.

With regard to CERN's test campaign of February 2017, two sets of activation measurements are of interest and reported in Table 2. For the tests, the reference value of 1.37E+08 $cm^{-2}s^{-1}$ was used since the most recent measurements shown an asymmetry which can be related to a misalignment of the foils.

Table 2 - Activation measurements at ILL-D50.

Foil	**Flux [$cm^{-2}s^{-1}$] P=55.8 MW November-2016**	**Flux [$cm^{-2}s^{-1}$] P=55.55 MW 25-January-2017**
A	1.26E+08	9.03E+07
B	1.18E+08	7.88E+07
C	1.37E+08	1.01E+08
D	1.26E+08	1.17E+08
E	1.31E+08	1.30E+08
AVERAGE	1.28E+08	1.03E+08

Beam profile can be assessed also by means of a neutron detector (Figure 14): an "Andor Ikon-L" CCD camera with 2048x2048 pixels and a pixel size of 13.5x13.5 μm was used together with a Zeiss Planar F100 mm lens (aperture F/2). The scintillation light was created through a ZnS/6LiF plate of 200x200x0.1 (0.2) mm. The neutron beam profile available in the highest flux position of D50 (characterized in this study) shows that it is homogeneous within 90% of the max intensity over an area of 15x15 mm^2 (see Figure 14).
D50 has a second irradiation area with an average neutron flux 3x lower but homogeneous over a larger area of around 25x25 mm^2. The maximum average flux at both position has been recently increased by a factor 4 after an upgrade of the instrument D50 including the reinforcement of the shielding (to be note that the term "instrument" refers to "facility").

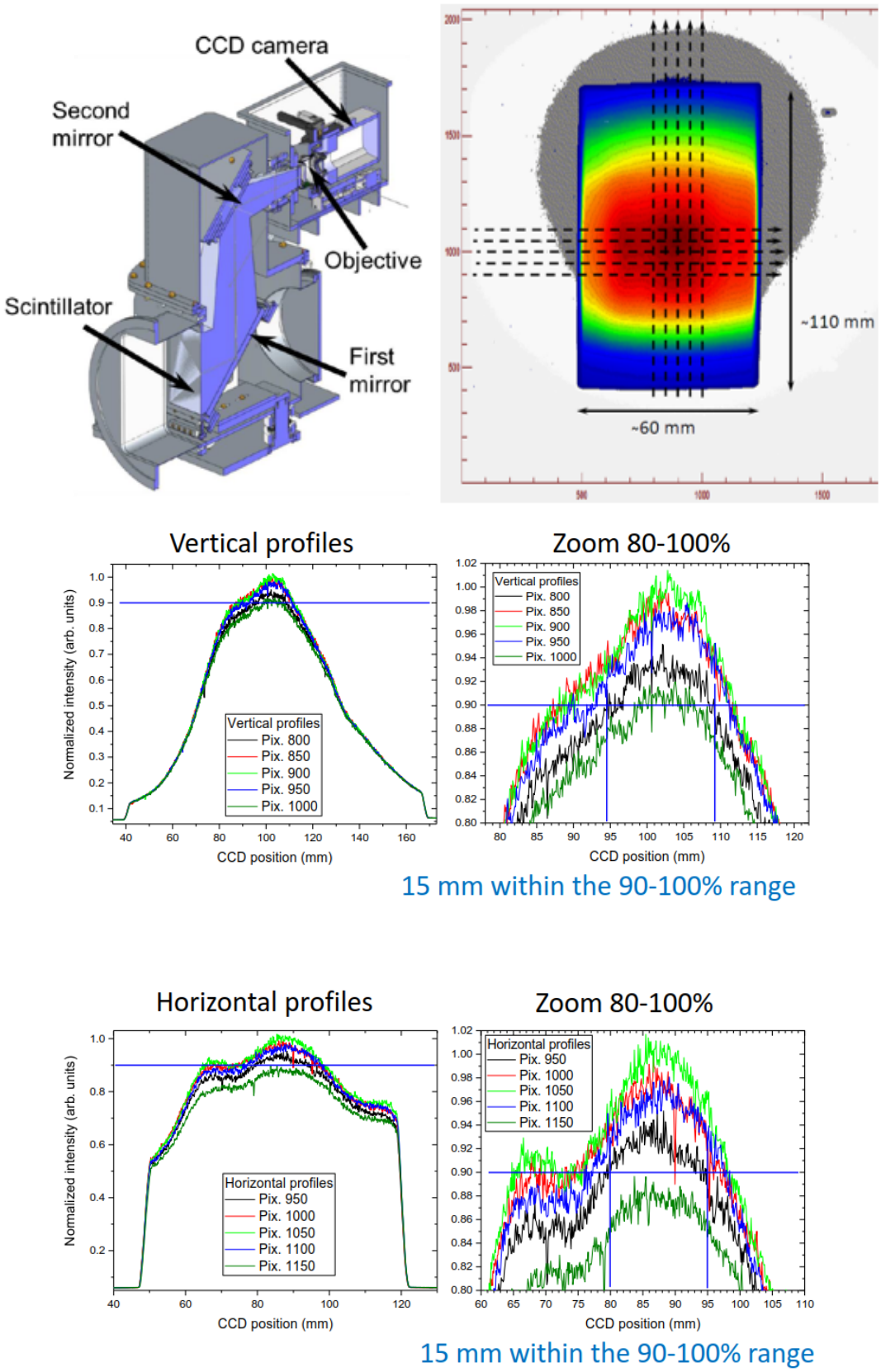

Figure 14 - CCD camera setup (Top left) used for the assessment of the beam profile (Top right, pixel units) at ILL-D50 with the respective beam profiles (Bottom). Every Pix. Curve corresponds to a different line on the beam profile.

3 Experimental setup

3.1 ESA Monitor SEU test setup

The ESA SEU Reference Monitor is a system developed by HIREX containing a chip module of 16 Mbit SRAM. Writing and reading are performed with a software provided by HIREX through an Ethernet connection with the board. Table 3 reports the main features of the two ESA monitors used in this test campaign whereas Figure 15 shows the typical experimental equipment used during and post-irradiation.

Name	Chip memory	Data code	Technology	Size	Data sheet Voltage [V]
ESA Monitor	AT68166F	1104	0.25 μm	16 Mbit	3.3 ± 0.3
ESA Monitor	AT68166H-YM20-E	1330	0.25 μm	16 Mbit	3.3 ± 0.3

Table 3 - ESA SEU Monitor specification

The standard equipment set for the test was composed by:

1) The ESA monitor board
2) Tue ESA Monitor 7.5V 2A DC power supply
3) Ethernet cables:
   30m long for LPSC (or using the Ethernet cable of the facility already present).
   10m long for ILL.

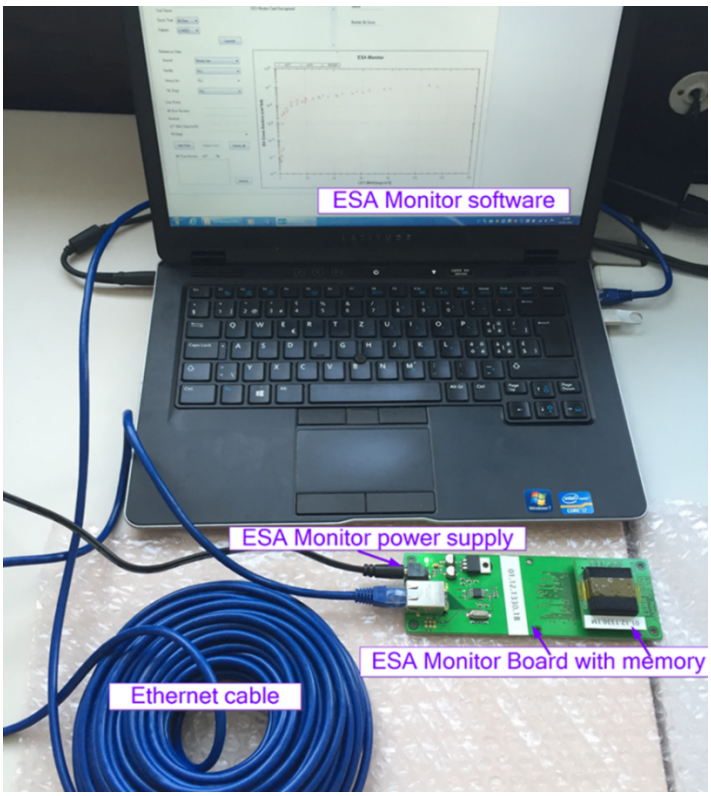

Figure 15 - ESA SEU Monitor setup.

The memory is made of 4 dies, as can be seen in Figure 16 and Figure 18. The lid can be removed to allow for a direct irradiation of the chips. The software (Figure 17) allows to write all the dies with a given pattern. In the tests presented here, the checkerboard pattern (CHKBD) was used, which means that the memory is written with consecutive 0's and 1's. At the end of the irradiation the memory was read to compare the data in each cell with the initial pattern: when the reference pattern does not

match with the post-irradiation one, the SEU counter is incremented. The number of errors in each die is displayed as well as their physical arrangement within the memory. The latter can be used to evaluate the particle flux homogeneity.

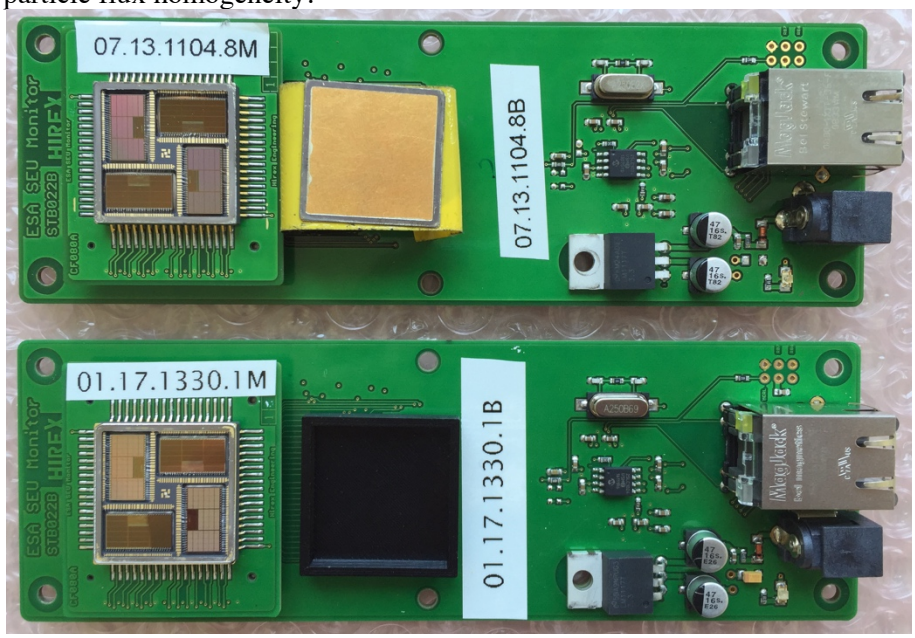

Figure 16 - ESA SEU Monitor boards, on the left the de-capsulated memories with the respective lid to the right. The upper board is the AT68166F 1104 and the bottom one is the AT68166H 1330.

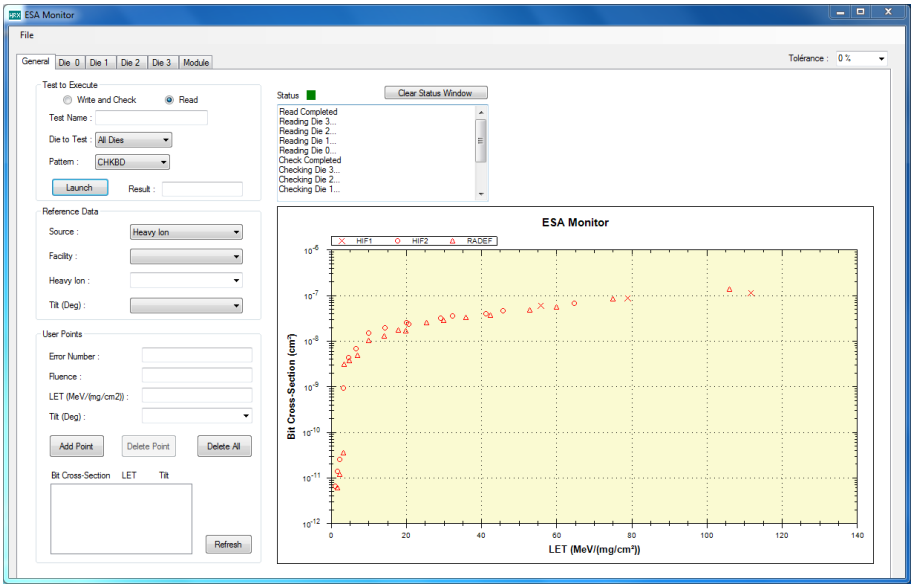

Figure 17 - ESA Monitor software

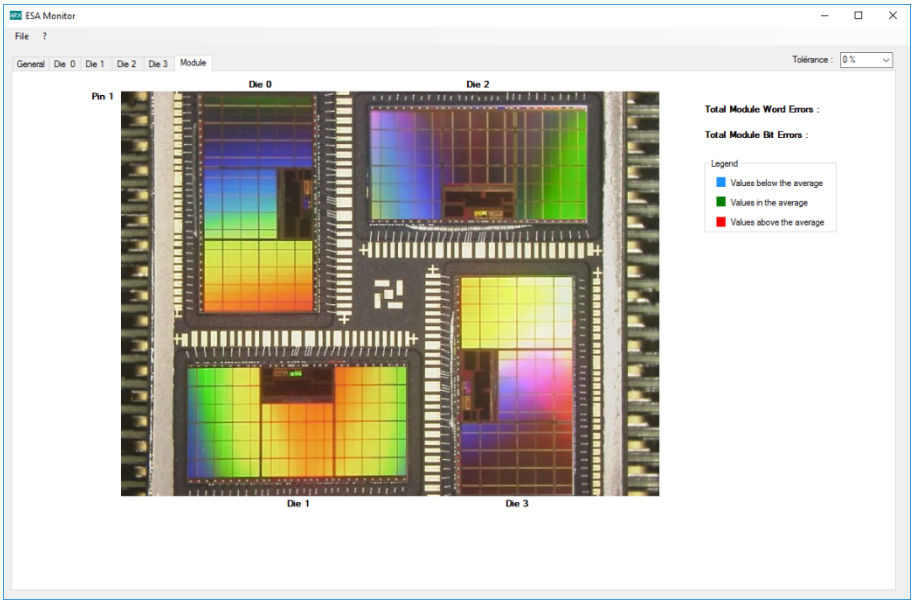

Figure 18 - ESA Monitor software: four dies disposition. The respective memory orientation is vertically with the power supply connector to the bottom.

The ESA Monitor was used in both LPSC and ILL, with the "center" of the memory (physical centre of the 4-die assembly) facing the beam. The positioning was performed by means of a laser beam (Figure 19): at LPSC, the positioning was done manually while ILL is equipped of remotely-movable slider for the horizontal (left-right) shifts with respect to the beam axis as depicted in Figure 20; up-down movements where done manually since, at the time, the facility could not provide of a remote control of vertical direction.

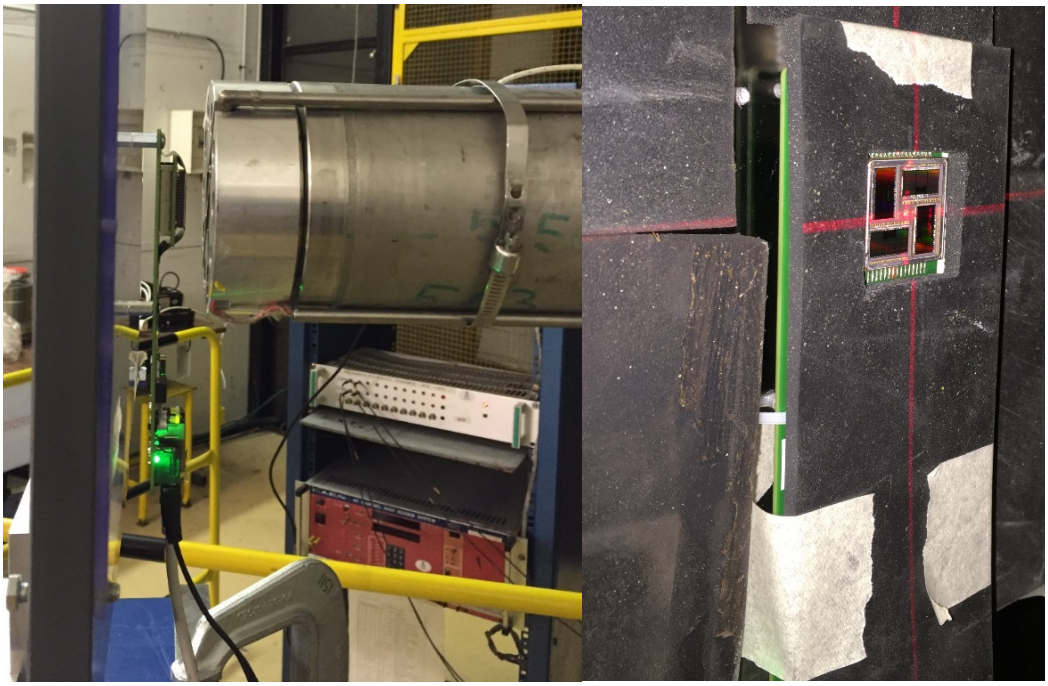

Figure 19 - ESA monitor on the support at LPSC (to the left) and ILL (to the right). In the latter, all the board except the active area was covered with boron carbide to minimise as much as possible the activation.

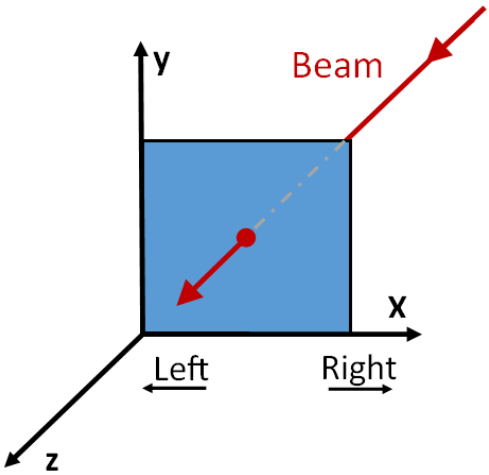

Figure 20 – Axis system reference (ILL).

3.2 Cypress SEU test setup

Two boards mounting a Cypress memory were tested in both the facilities to evaluate the SEU sensitivity (Figure 21). The reading of the memory was performed with a serial data communication by means of a USB-Ethernet-USB cable and the Docklight software for the communication with the laptop: this software allows to read the memory in real-time every second as can be seen in
Figure 22, where the hexadecimal values are the upsets referred to each second. The output data are the SEU number (in this case expressed in hexadecimal format) occurred in 1 second in the memory, so that every second the memory was read and the SEU counter resets. The final SEU number is obtained summing all the events. Table 4 reports the main features of the Cypress memories used in this test campaign.

Name	Chip memory	Data code	Technology	Size	Data sheet Voltage [V]
Cypress	CY62157EV30LL-45ZSXI	1443	90 nm	512Kx16	2.20 ÷ 3.60
Cypress	CY62157EV30LL-45ZSXI	1437	90 nm	512Kx16	2.20 ÷ 3.60

Table 4 - Cypress specifications.

Cypress setup equipment:

1) Cypress board with its supply connector
2) Female pins connector to USB (for the serial communication)
3) 2 x Ethernet to USB extender
4) 2 x BNC to BNC male cable + 4 x BNC female to banana adaptor
5) 30m long for LPSC (otherwise two BNC-BNC male cables are already present)
6) 10m long for ILL
7) Keysight power supply E3648A
8) Laptop with Docklight software

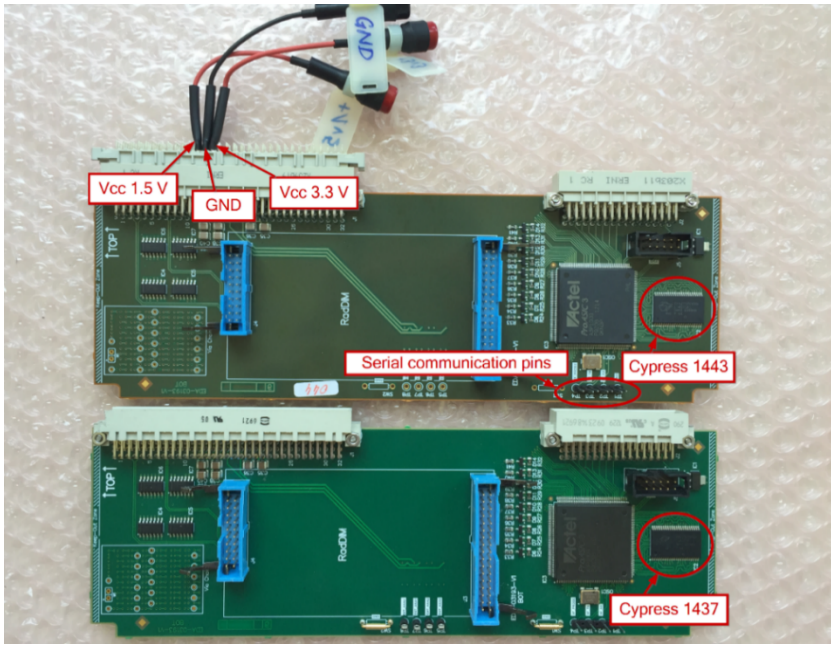

Figure 21 - SRAM Cypress CY62157EV30LL-45ZSXI boards with two different data code 1443 and 1437.

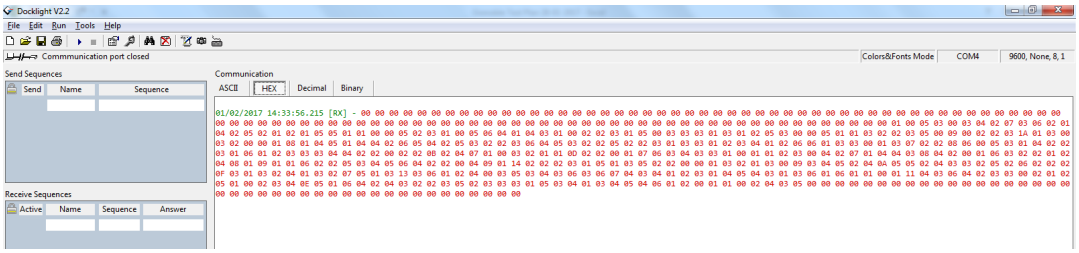

Figure 22 - Docklight software for the memory reading. The transmission of the data is conducted by means of a serial data communication.

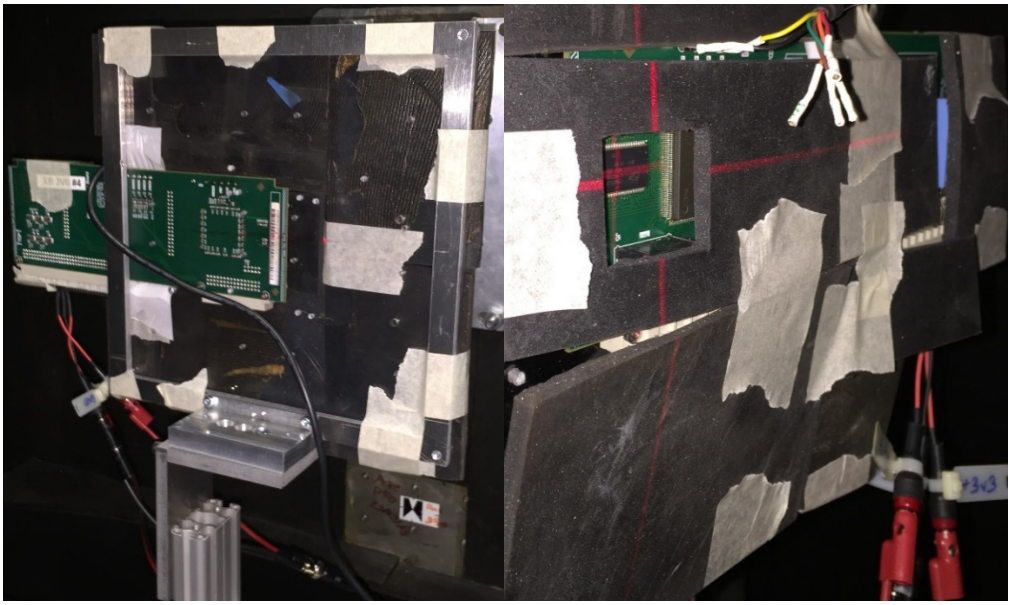

Figure 23 - Laser centring of the Cypress memory (to the right) and back view of the support and the board (to the left) at ILL facility. The black material that cover the board except the memory is boron carbide.

3.3 SEL tests setup

For the SEL tests, COTS memories from different manufacturers were employed. The test boards, developed at CERN, have two inputs, namely ground and Vcc. The boards house 8x chips soldered on it except for the Brilliance 11254 that was tested as a single chip. Table 5 reports the main features of the memories used for the SEL tests.
The equipment needed for the test is:

1) Memory boards
2) Keysight power supply E3648A
3) 1 x BNC to BNC male cable + 2 x BNC female to banana adaptor
   30m long for LPSC (a BNC-BNC male cable is already present in the facility)
   10m long for ILL.
4) Laptop with PS Control
5) GPIB to USB connector
6) Digital multimeter to verify the voltage drop on the cable

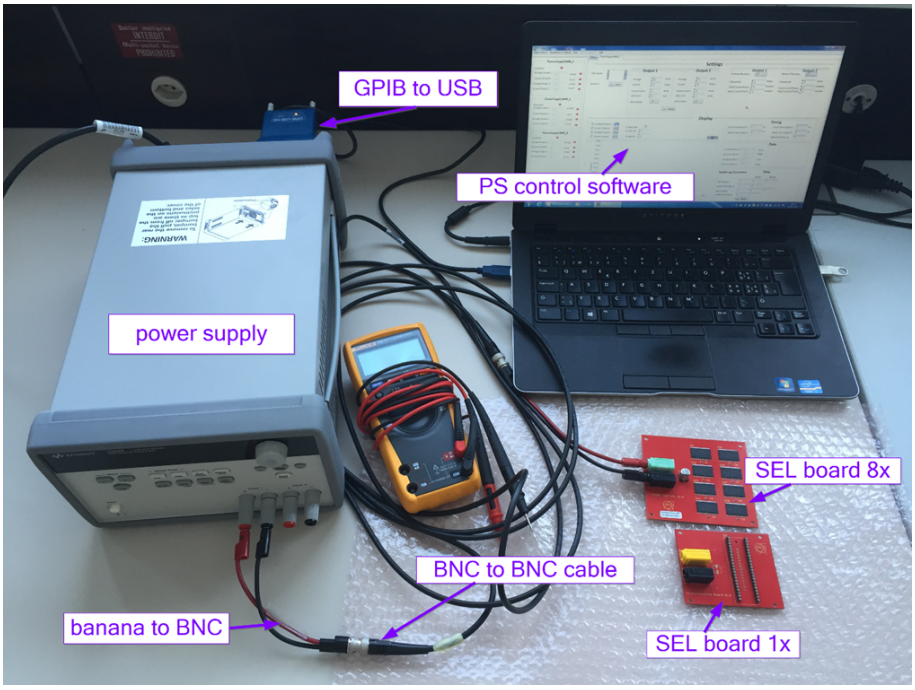

Figure 24 - SEL setup.

Name	Part Number	Data code	Technology	Size	Data sheet Voltage [V]
ISSI	IS61LV5128AL-10TLI	1246,1303	0.18 μm	512K x 8	3.3 ±10%
Brilliance	BS62LV1600EIP55	12094	0.18 μm	2M x 8	2.4 ÷ 5.5
Brilliance	BS62LV1600EIP55	11254	0.18 μm	2M x 1	2.4 ÷ 5.5
Lyontek	LY62W20488ML-55LL	1251	0.18 μm	2048K x 8	2.7 ÷ 5.5

Table 5 – SEL-tested memories: main features.

Figure 25: SEL-tested memories: ISSI 1246 (Left), Brilliance 12094 (centre), Lyontek 1251 (Right)

For the Brilliance and Lyontek memories, each board had 8 chip of memory with the same date code, only the ISSI memories had 2 different date codes. To distinguish one board from the other an identification label was placed in order to identify possible board-to-board sensitivity spread.

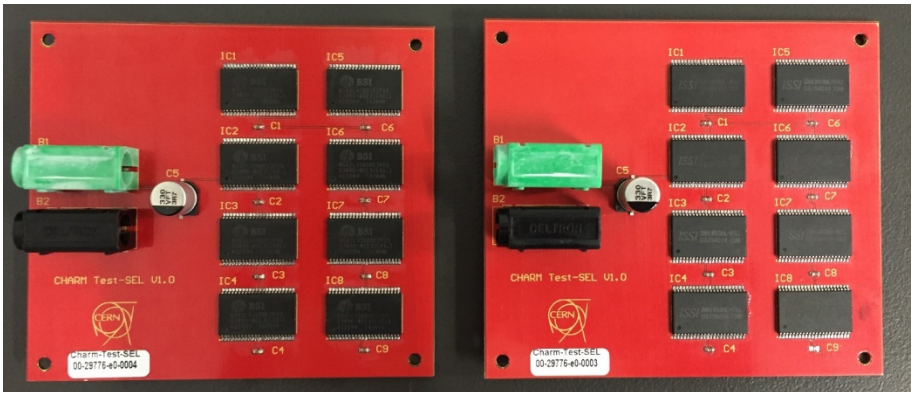

Figure 26 - Brilliance and ISSI 8x memory boards (Lyontek has also the same base board)

The boards were connected with a banana-BNC cable to a power supply: a KEYSIGHT E3648A. This device can be controlled with a computer by means of the GPIB-USB-HS controller using a LabVIEW software "PsControl" (Figure 28). This program can count the number of SELs that occur in the memories. There are three main input parameters to detect and reset an SEL, as illustrated in Figure 27:

1. the current threshold (Ithres),
2. the hold time (thold),
3. the cut time or reset time (tcut).

If the current consumption of the component is above the current threshold during the hold time an SEL was occurred. Therefore, the voltage is set to 0V and it lasts for the cut time. Finally the component is powered up again.
Usually (thold + tcut) lasts about 1.5 seconds. As SELs are separated from a minimum mean of 35 seconds, it is rather unlikely that SEL detection and reset time can overlap to the next latch-up, therefore the associated detection dead-time can be neglected

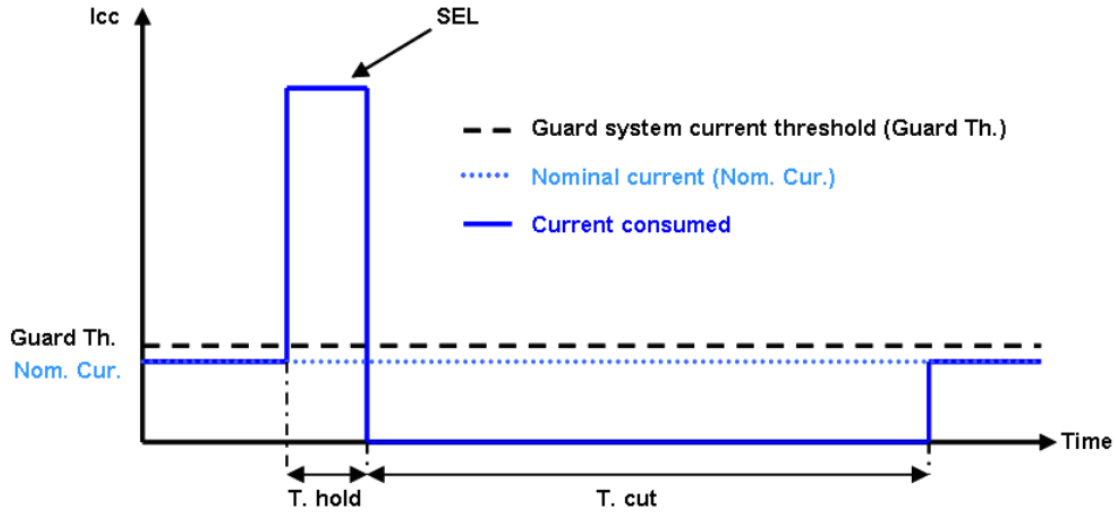

Figure 27 – SEL detection: typical cycle

Table 6 shows the main settings in the PS Control LabVIEW software for the currents and voltage. For the ISSI memory a voltage of 3.67V was applied due to the voltage drop on the cables, so that the board was powered to 3.3V. A similar case applies for the Alliance.

Table 6 - SEL parameters on PS control, Voltage, Current and Ithres are these set in the software.

Component	**Voltage(V)**	$I_{nominal}$ (A)	***Current limit (A)***	***I_{thres}(A)***
ISSI 8x	3.3	0.265	***0.5***	***0.3***
Brilliance 8x	3.3	0.01	***0.05***	***0.02***
Lyontek 8x	3.3	0.005	***0.05***	***0.02***
Brilliance 1x	3.3	0.003	***0.05***	***0.02***

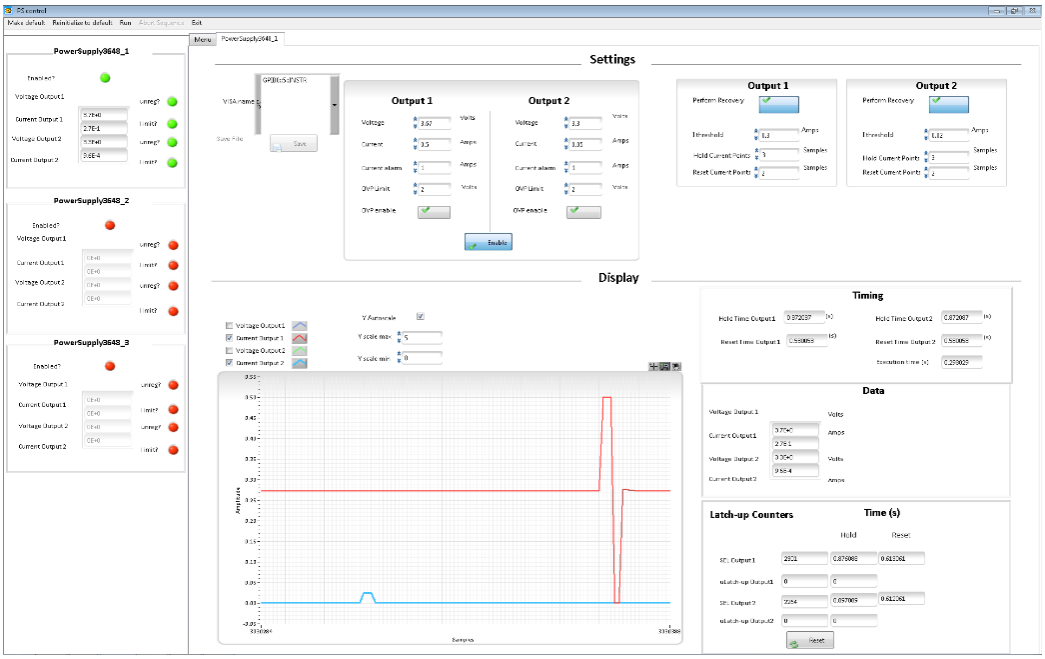

Figure 28 - LabVIEW PS control software showing an SEL event, the program show in real time the evolution of current (blue) and voltage (red) for both the channel.

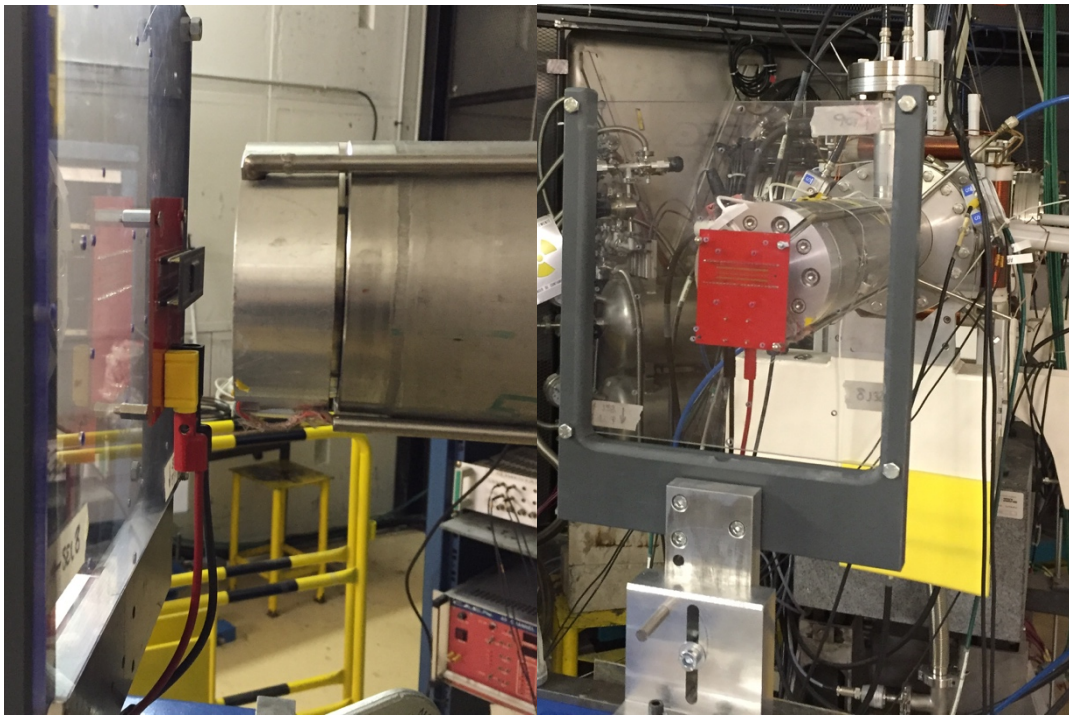

Figure 29 – 8 x ISSI board (to the left) and 1xBrilliance memory (to the right) at LPSC.

4 Flux and homogeneity cross-calibration with the ESA Monitor

Before conducting the tests, a cross-calibration of both LPSC and ILL facilities was performed to assess the position and homogeneity of the beam. The general formula to retrieve the flux is the following:

$$\dot{\phi} = \frac{N_{SEU}}{\Delta t \times \sigma_{ref} \times n_{bit}} \left[\frac{\mathrm{n}}{\mathrm{cm}^2 s}\right]$$

Equation 1 – ESA Monitor flux calculation.

Where N_{SEU} is the measured upset number, Δt the irradiation time, σ_{ref} the reference cross section and n_{bit} the bit number which the memory is composed of.

4.1 LPSC calibration

Using the experimental setup described above, the ESA Monitor #1 with reference AT68166H-YM20-E and date code 1330 was irradiated for different irradiation times and at different distances as summarized in Table 8. The distance is relative to the center of the target source so that the outer surface is placed 24 mm onwards. For example, placing the memory at 25 mm is equivalent to saying that the memory was at 1 mm from the outer surface of the machine. The distances were manually set with the aid of a ruler. The reference cross section (highlighted in yellow in Table 7, 8 and it has to be noted that this is not an interaction cross section) is calculated as follows:

$$\sigma = \frac{N_{SEU}}{\phi \times n_{bit}} \left[\frac{\mathrm{cm}^2}{\mathrm{bit}}\right]$$

And the fluence value

$$\phi = \Delta t \times \dot{\phi}_{ref} \times \frac{I}{I_{ref}} \times \left(\frac{d_{ref}}{d_i}\right)^2 \quad \left[\frac{\text{n}}{\text{cm}^2}\right]$$

Equation 2 – Fluence calculation (LPSC).

where Δt is the test time, $\dot{\phi}_{ref}$ = 3.2E+07 $cm^{-2}s^{-1}$ is the reference flux at 34 mm provided by the facility for a reference current $I_{ref} = 120\ uA$ and I the average intensity measured current during the test. In this case, there is no dependence with the distance because the fluence is that of reference at 34 mm. The cross section uncertainty was computed by a quadratic uncertainty propagation, i.e. considering three uncertainty contributes: the test time (0.3%), the average current (9%) and the reference flux uncertainty (4%).

Data code	Current [uA]	Distance [mm]	Test time [s]	Fluence [n/cm²]	SEU	σ [cm²/bit]	% σ error
1330	145	34	331	1.28E+10	5363	2.49E-14	9.5

Table 7 – ESA SEU Monitor reference cross section.

Considering the previous cross section $\sigma_{ref} = 2.49E-14\ [\frac{\text{cm}^2}{\text{bit}}]$ (Table 7) as reference, since the flux provided by the facility refers to this position, the ESA Monitor measured fluxes are retrieved from Equation 1, with $n_{bit} = 2^{24}$ the overall bit number of the 4 ESA Monitor dies. However, the cross section obtained at PTB with 14.8 MeV neutrons resulted of $\sigma_{ref} = 2.22E-14\ [\frac{\text{cm}^2}{\text{bit}}]$ but using the reference AT68166F (1036) [19].

As the flux is inversely proportional to the square of the distance between the reference point and the other, the theoretical flux was calculated for a comparison with that of the ESA Monitor:

$$\dot{\phi}_{th}(d_i) = \dot{\phi}_{refEM} \left(\frac{d_{ref}}{d_i}\right)^2 \left[\frac{\text{n}}{\text{cm}^2 s}\right]$$

$$\dot{\phi}_{refEM} = 3.88E+07 \quad \left[\frac{\text{n}}{\text{cm}^2 s}\right]$$

Data code	Current [uA]	Distance [mm]	Test time [s]	SEU	E.M. flux [cm⁻²/s]	Theoretical flux [cm⁻²/s]	% flux
1330	139	25	152	3872	6.10E+07	7.17E+07	15.0
1330	145	34	331	5363	3.88E+07	3.88E+07	0.0
1330	143	44	420	4260	2.43E+07	2.32E+07	-4.8
1330	136	54	300	1981	1.58E+07	1.54E+07	-2.8
1330	138	74	608	2244	8.83E+06	8.19E+06	-7.9

Table 8 – ESA SEU Monitor (E.M.) results (AT68166H-YM20-E reference board without the lid). Highlighted in yellow, the reference cross section for calculating the flux at different distance.

From the values of Table 8 it is possible to compare the measured neutron flux profile as a function of the distance with the neutrons flux provided by the facility (Figure 30): the two curves resulted in an excellent agreement within the 8%. The only point with a 15% of mismatch is that at 24 mm from the source center (only 1 mm from the source output) where small uncertainty in the positioning can lead to significant uncertainty in the flux assessment. Due to the manual positioning of the memory during these tests and the objective difficulty in assessing a proper uncertainty value this aspect was not included in the total uncertainty calculation. Since then, a remotely motorized system has been installed at the facility to position precisely the DUT.

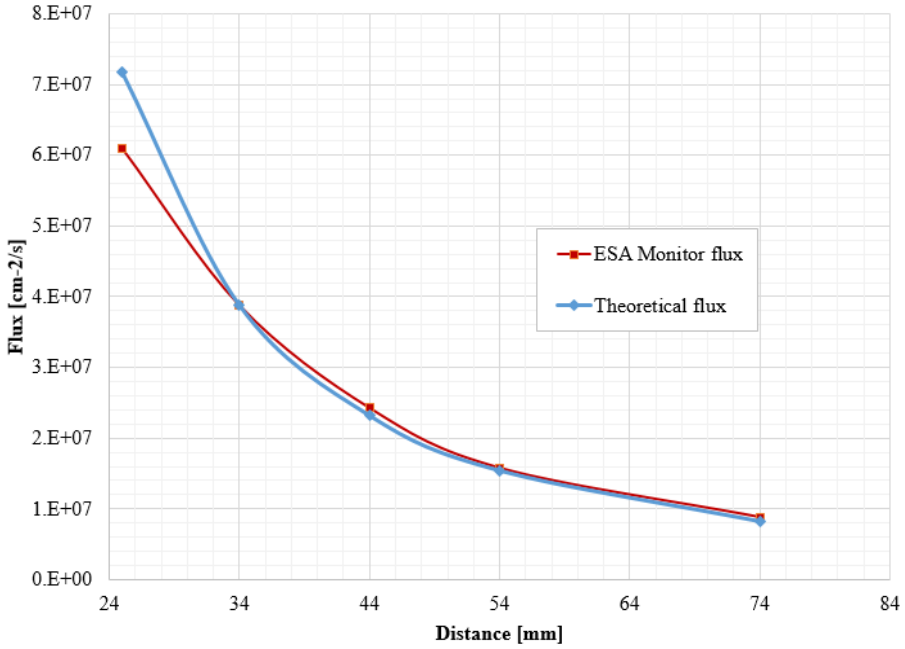

Figure 30 - ESA Monitor flux vs distance from the center of the source, compared with that is inversely proportional to the square of the distance.

The beam homogeneity was checked using the ESA Monitor software as shown in Figure 31. Considering that the active area of the memory is 20 x 20 mm (from the start of the die0 to the end of the die2), looking at the SEU counts (red) it's clear that they are uniformly distributed in all the surface of the dies. Hence the LPSC 14 MeV beam can be considered as homogeneous. The homogeneity evaluation was performed at all the distances (not included in this report) in which the tests were conducted: as for the 34 mm case, an overall satisfactory homogeneity was found.

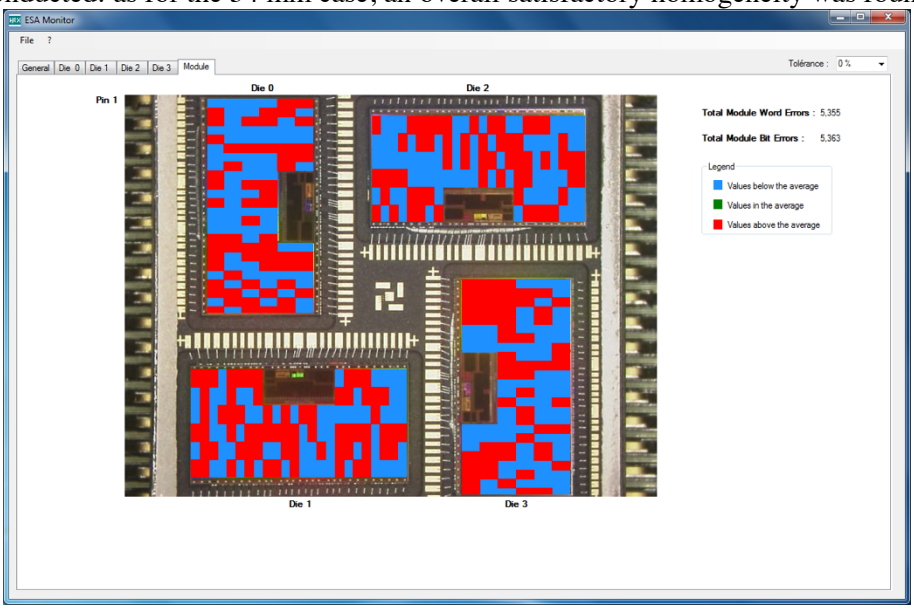

Figure 31 - ESA SEU Monitor software showing the beam homogeneity at 34 mm, in red the occurred SEU.

4.2 ILL calibration

Similarly to LPSC, the same ESA Monitor type was used at the ILL D50 instrument for the calibration and homogeneity check before testing other components.

The ESA monitor was mounted on a dedicated support which was moved in the left-right direction through the system described in Figure 20. For all the tests the AT68166H-YM20-E reference memory was employed without the plastic lid. The measurements were performed in 11 positions by moving the support to the left, right, up and down; the distance between the memory and the neutron nozzle was fixed. Every run lasted "Test time Δt_i" and the thermal neutron flux considered at the centre of the beam was that provided from the facility as described in section 2.1.2.
Table 9 reports the SEU results at different distances from the center. Since the ESA Monitor has a different area (a square of 20 x 20 mm) with respect to that of the foil calibration (a circle of 10 mm diameter), for geometric considerations the flux that crosses the ESA Monitor surface is considered to be the same quantity that passes through all the five foils. Therefore it is calculated as the arithmetic mean of the five calibration fluxes and it is equal to 1.28E+08 $cm^{-2}s^{-1}$. To compute the fluxes in all the other positions, the reference flux was scaled with the SEU number and measurement time of the test 1.

$$\dot{\phi}_i = 1.28E8 \times \frac{SEU_i}{SEU_{ref}} \times \frac{\Delta t_{ref}}{\Delta t_i} \left[\frac{\text{n}}{\text{cm}^2 s}\right]$$

Fluxes and cross section are calculated in Table 9.

Test	Data code	Setup	Position [mm]	Test time [s]	Flux 1 [n/cm2/s]	SEU	$\sigma 1$ [cm2/bit]
1	1330	no lid	c	300	1.28E+08	2907	4.51E-15
2	1330	no lid	c + 3 mm left	300	1.26E+08	2858	
3	1330	no lid	c + 3 mm left	300	1.24E+08	2808	
4	1330	no lid	c + 13 mm left	180	1.22E+08	1666	
5	1330	no lid	c + 23 mm left	180	1.02E+08	1392	
6	1330	no lid	c + 33 mm left	180	4.35E+07	593	
7	1330	no lid	c + 43 mm left	181	5.91E+06	81	
8	1330	no lid	c + 7 mm right	180	1.21E+08	1645	
9	1330	no lid	c + 17 mm right	180	1.07E+08	1460	
10	1330	no lid	c + 27 mm right	180	6.88E+07	937	
11	1330	no lid	c + 21 mm up	181	1.23E+08	1687	
12	1330	no lid	c + 21 mm down	186	5.62E+07	792	

Table 9 – ESA SEU Monitor AT68166H-YM20-E measurements in different positions. c = center and left or right are referred as if the observer is seeing the upcoming beam in front of him (Figure 20).

In the test number 1 the ESA Monitor active area was placed with respect to the reference system of the facility (see Figure 20), with the beam centered on the middle of the 4 dies. As shown in Figure 32, the beam was quite inhomogeneous given that the dies 2 and 3 recorded 60% and 30% more upset with respect to the dies 1 and 0.

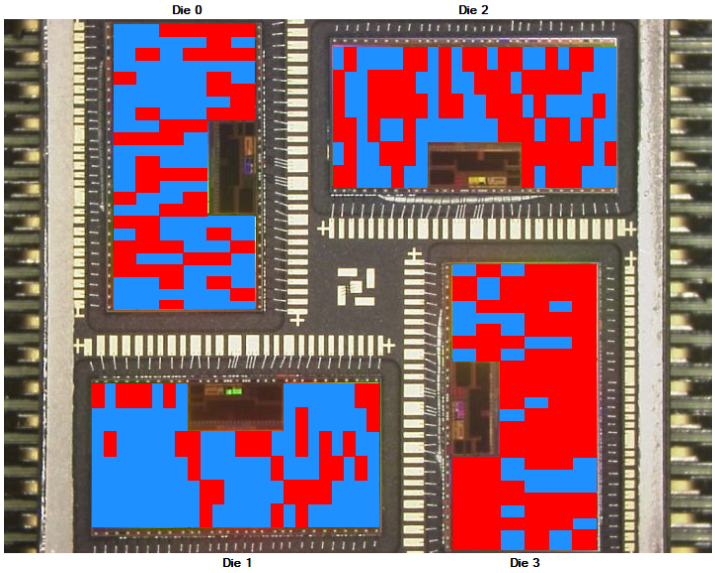

Figure 32 – ESA monitor events for the centered run: in red are indicated the SEU.

All the other measurements were done considering the center at 3 mm toward the left (from the test 2 to the test 10). The ratio between the SEU of die3 and those of the die0 is expected to be close to 1 for a perfect homogeneity and as shown in Table 10, the position at 23 mm to the left from the center comes closest to the SEU symmetry on the dies.

Test	Position [mm]	die0	die1	die2	die3	die3/die0	die2/die1
1	c	637	538	707	1025	1.61	1.31
2	c + 3 mm left	624	613	696	925	1.48	1.14
3	c + 3 mm left	625	569	691	923	1.48	1.21
4	c + 13 mm left	359	380	374	553	1.54	0.98
5	c + 23 mm left	352	296	314	430	1.22	1.06

Table 10 – ESA Monitor SEU of each die.

A quick overview of the left shifts (test number 4, 5, 6, 7) is reported in Figure 33 where the best homogeneity was found for test 5 at 23 mm toward the left, and after this position the memory started to exit from the beam area.

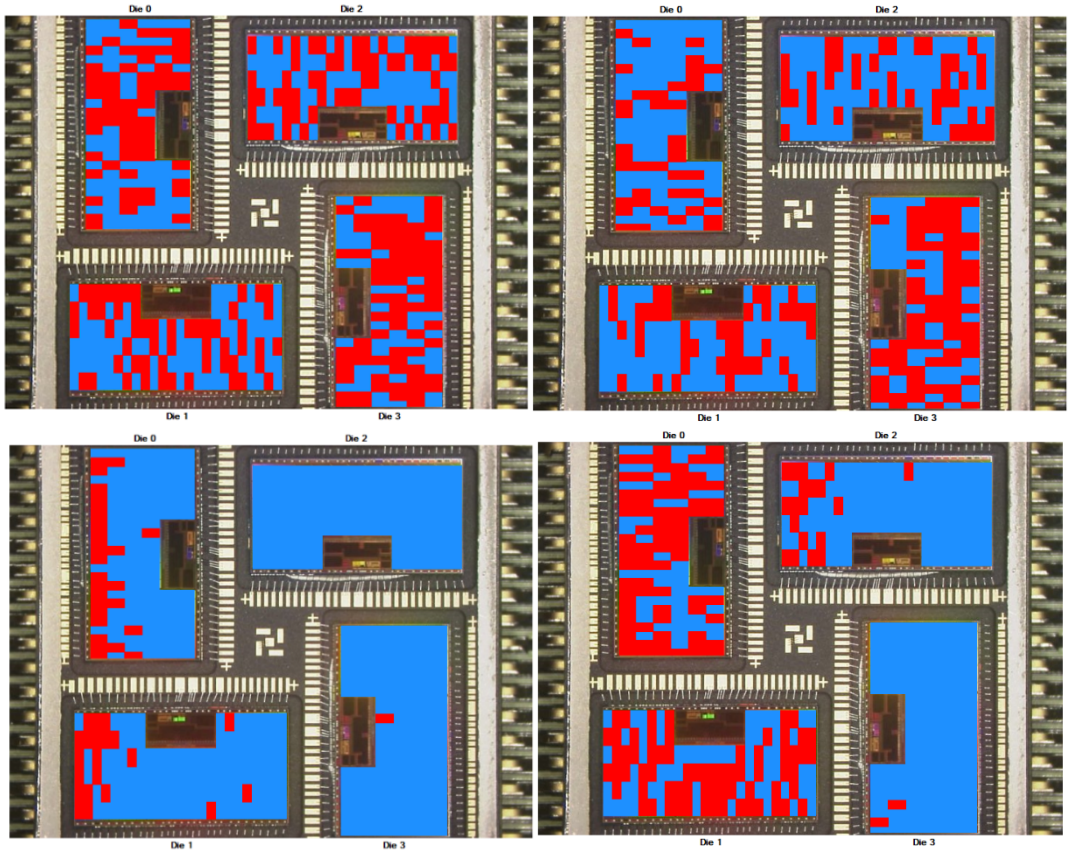

Figure 33 - ESA Monitor events; the following distance refers to the left shift of the memory: at 13 mm on the top-left, 23 mm on the top-right, 43 mm on the bottom-left, 53 mm on the bottom-right picture. Respectively the tests number 4,5,6,7.

A possible explanation of this observation could be that the real beam center was shifted toward the left and therefore to the right of the picture in Figure 32 for the horizontal axis. The 2 cm shift between the beam nozzle and the memory support, amounts to a beam offset within 2-3 degrees toward the left.
Regarding the ESA Monitor, the equation $N_{SEU} = \sigma \times \phi$ is valid either if the memory have been irradiated with a homogeneous flux or the total fluence, retrieved from an inhomogeneous flux, it is known. Since the reference flux provided by the facility covers only the center C for the ESA monitor measurements and, as explained before, the mean flux for this position can be obtained averaging the 5 given fluxes, the ESA monitor thermal neutron cross section results 4.51E-15 cm^2/bit.
The previous reference value was measured in Orphée for the same technology and reference memory but for a different data code: the cross section value was 3.3E-15 cm^2/bit [20].
In Figure 34 the ESA Monitor flux calibration are compared with that of the facility displayed to the top-right of the same figure. The beam center C has been considered the center + 3 mm to the left. The fluxes expressed in neutron $cm^{-2}s^{-1}$ are calculated from Equation 1 considering the ESA Monitor cross section of:

Test 2[2], σ = 4.51E-15 cm^2/bit

Each square represents the total ESA Monitor active area, 20 x 20 mm^2. On the green area, C is the center (test 2), A and E the up and down measurements (test 11 and 12), B and D the left and right ones (test 5 and 9). By normalizing all the different tests by the central value C, we obtain the values reported in the yellow squares, which allow a direct comparison with the facility calibration. It is important to underline that the active areas are different: indeed the activation foils used in the facility

[2] Note that this is the value at 3 mm to the left from the facility center. It has been used for symmetric reason of the measurements.

calibration are 10 mm in diameter so that the comparison is only qualitative. With the ESA Monitor dimensions, the beam intensity to the bottom is half with respect to the center whereas on the other side the intensity decreasing is lower and almost unchanged on the top.

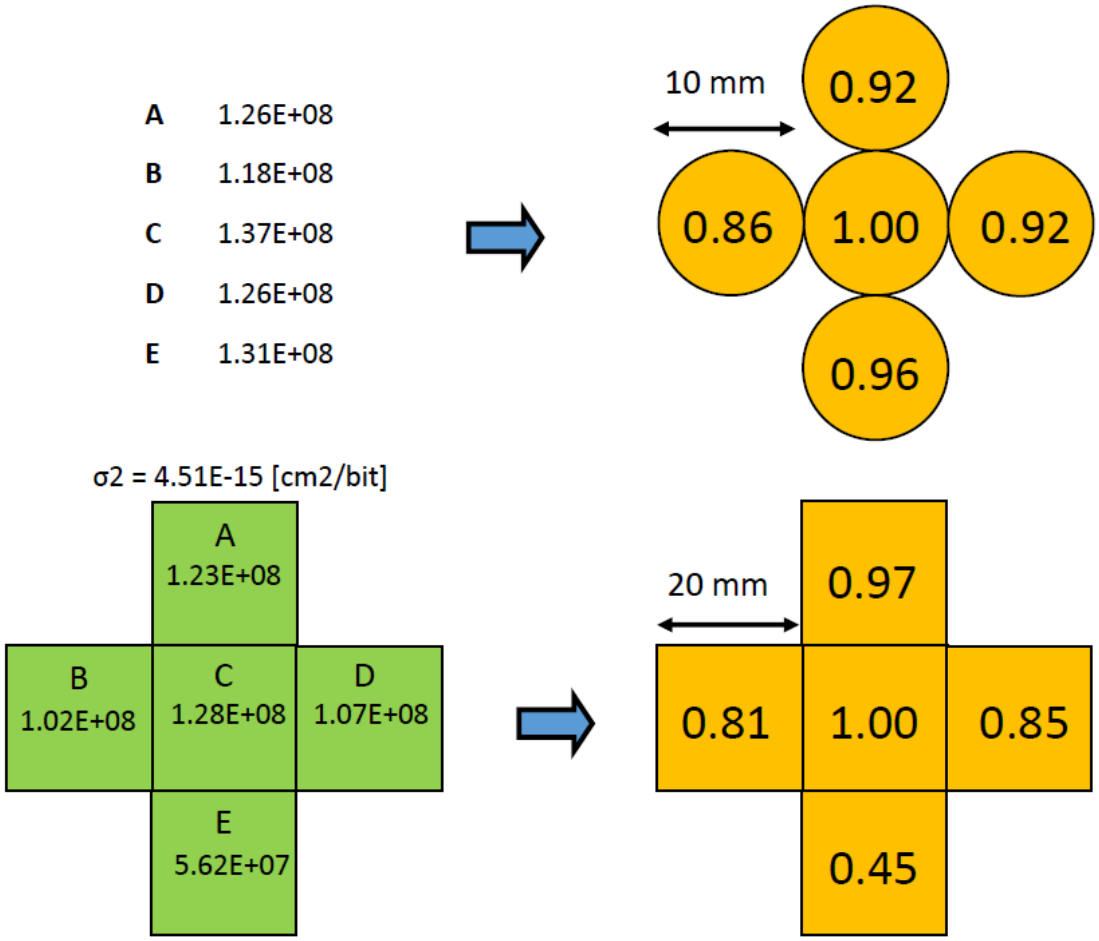

Figure 34 – To the left the ESA Monitor flux calibration [n/cm2/s] (in green) with below the corresponding normalized values with respect to the center C, in comparison with the golden foil calibration of the facility to the right.

Overlaying the normalized ESA monitor and gold-foil flux calibration, the covered area is reported in Figure 35.

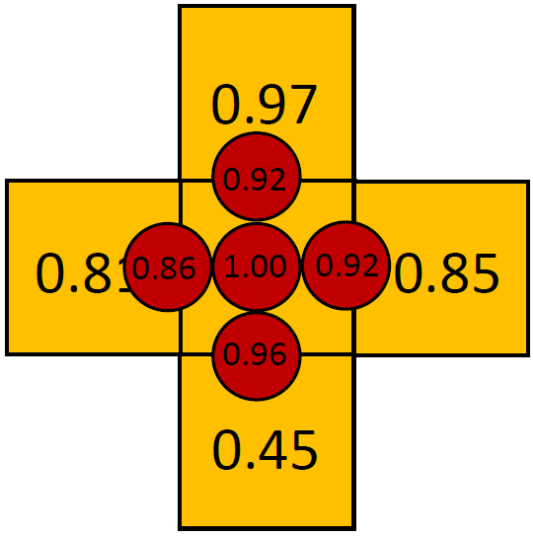

Figure 35 - ESA Monitor (in yellow) and gold foil (in red) flux calibration.

In conclusion, the center "c" of the beam provides the maximum mean intensity but from the ESA Monitor measurement the homogeneity over the area of 20 x 20 mm varies up to 60% (Table 10) whereas, from the facility calibration (from Figure 14) the intensity ranges of about 13% considering the same area. However, the comparison is only qualitative because this ESA Monitor assessment relies on the ratio between the SEUs on the dies. By moving 23 mm toward left of the center "c", the flux appears homogeneous but with half of intensity with respect to the center. The intensity decreasing is symmetric in the horizontal axis whereas differs of a factor two in that vertical (Figure 35). Therefore, it can be concluded that at the location designated as beam centre by the facility, the flux assessment by means of the ESA Monitor is not homogeneous over a surface (20 x 20 mm^2), typically characteristic of micro-electronic components.

5 Test results

The results are gathered on the basis of the facility (LPSC or ILL) and the type of Single Event Effect (Upset or Latch-up). For completeness also the ESA Monitor cross sections are reported in this section and the detailed analysis can be found in the above chapters concerning the calibration check of the facilities. The different type of SRAM memories tested in this experimental campaign are listed in Table 11.

Memory	Reference	Label	Data code	Technology
ESA Monitor	AT68166F	8	1104	0.25 μm
ESA Monitor	AT68166H-YM20-E	1 and 2	1330	0.25 μm
Cypress (prototype)	CY62157EV30LL-45ZSXI	-	1443	90 nm
Cypress	CY62157EV30LL-45ZSXI	-	1437	90 nm
Brilliance x1	BS62LV1600EIP55	BSI-XI-2	11254	0.18 μm
ISSI x8	IS61LV5128AL-10TLI	00-29776-e0-0002	1246, 1303	0.18 μm
Lyontek x8	LY62W20488ML-55LL	00-29222-e1-0003	1251	0.18 μm
Brilliance x8	BS62LV1600EIP55	00-29776-e0-0005	12094	0.18 μm

Table 11 – Tested SRAM memory at ILL or/and LPSC. The Brilliance and Lyontek memories have been tested at 3.3 and 5.5 V.

For both SEL and SEU experiments, when less than 50 events were counted, the upper limit of the cross section was calculated using a Poisson distribution with 95% of confidence level, as reported in [21]. These values are shown in Table 12.

N	95% Limits lower	upper	N	95% Limits lower	upper	N	95% Limits lower	upper
0	0.0	3.7	17	9.9	27.2	34	23.5	47.5
1	0.1	5.6	18	10.7	28.4	35	24.3	48.7
2	0.2	7.2	19	11.5	29.6	36	25.1	49.8
3	0.6	8.8	20	12.2	30.8	37	26.0	51.0
4	1.0	10.2	21	13.0	32.0	38	26.8	52.2
5	1.6	11.7	22	13.8	33.2	39	27.7	53.3
6	2.2	13.1	23	14.6	34.4	40	28.6	54.5
7	2.8	14.4	24	15.4	35.6	41	29.4	55.6
8	3.4	15.8	25	16.2	36.8	42	30.3	56.8
9	4.0	17.1	26	17.0	38.0	43	31.1	57.9
10	4.7	18.4	27	17.8	39.2	44	32.0	59.0
11	5.4	19.7	28	18.6	40.4	45	32.8	60.2
12	6.2	21.0	29	19.4	41.6	46	33.6	61.3
13	6.9	22.3	30	20.2	42.8	47	34.5	62.5
14	7.7	23.5	31	21.0	44.0	48	35.3	63.6
15	8.4	24.8	32	21.8	45.1	49	36.1	64.8
16	9.4	26.0	33	22.7	46.3	50	37.0	65.9

Table 12 Poisson distribution margin limits with 95% of confidence margin.

The cross section, normalized by bit or chip for SEU and SEL respectively, were calculated as follows:

$$\sigma = \frac{N_{SEU}}{Fluence \times n_{bit\ or\ chip}} \left[\frac{\text{cm}^2}{\text{bit or chip}}\right]$$

Only the fluence calculation varies according to the facilities as expressed below.

5.1 LPSC

The fluence values are retrieved from Equation 2, where Δt_i is the test time, $\phi_{ref} = 2.2E7 \left[\frac{n}{cm^2 s}\right]$ the reference flux, I_i the measured current and $I_{ref} = 120\ uA$ the reference current provided by the facility. The cross section errors are retrieved as in the LPSC calibration section, as well as the uncertainty.

SEU tests

Memory	Reference	Data code	Setup	Current [uA]	Distance [mm]	Test time [s]	Fluence [n/cm2]	SEU	σ [cm2/bit]	% σ error
ESA Monitor	AT68166F	1104	no lid	134	34	300	1.07E+10	4349	2.43E-14	12.3
ESA Monitor	AT68166F	1104	no lid 180°	127	44	150	3.04E+09	480	9.42E-15	15.6
ESA Monitor	AT68166H-YM20-E	1330	no lid	145	34	331	1.28E+10	5363	2.49E-14	9.5
Cypress (prototype)	CY62157EV30LL -45ZSXI	1443	-	130	54	392	5.38E+09	3072	6.81E-14	13
Cypress (prototype)	CY62157EV30LL -45ZSXI	1443	180°	123	54	360	4.70E+09	1145	2.91E-14	14

Table 13 – SEU tested SRAM memories at LPSC 14 MeV neutrons.

SEL tests

Memory	V	Current [uA]	Distance [mm]	Test time [s]	Fluence [n/cm2]	SEL	σ [cm2/chip]	% σ error
Brilliance x1	5.5V	124	54	1800	2.36E+10	50	2.11E-09	±16.5
Brilliance x1	3.3V	123	54	1380	1.79E+10	0	<2.06E-10	-
ISSI x8	3.3V	148	44	1216	2.91E+10	1	<2.41E-11	-
Lyontek x8	5.5V	137	44	1200	2.92E+10	10	<7.88E-11	-
Lyontek x8	3.3V	133	44	1200	2.83E+10	5	<5.16E-11	-
Brilliance x8	5.5V	150	44	1200	2.62E+10	33	<2.21E-10	-
Brilliance x8	3.3V	153	44	1200	2.55E+10	22	<1.63E-10	-

Table 14 – SEL tested SRAM memories at LPSC 14 MeV neutrons.

Noteworthy is the fact that whereas the Brilliance 8x powered with 3.3V recorded two-third of SEUs compared with those of the same memory but supplied with 5.5V, the Brilliance 1x recorded zero events at low voltage 3.3V and 50 at 5.5V. This could be associated to the fact that they have two different data code, respectively 12094 (8x) and 11254 (1x) and the behaviour as a function of the voltage is very different.
Moreover, the SEU cross sections are reduced by a factor 2-3 when the memories are rotated of 180 degrees and irradiated on the back part. This is attributed to the neutrons that interact with oxygen in the Back End of Line (BEOL) and the latter recoil with a larger energy and LET than silicon due to its lighter nature [22] [23].

5.2 ILL

The fluence is the product of the flux by the test time:

$$\phi_i = \Delta t_i \times \dot{\phi}_i \left[\frac{\mathrm{n}}{\mathrm{cm}^2}\right]$$

According to [21] the cross sections relative errors are calculated taking into account the Poisson distribution where the standard deviation is the square root of the events. In particular:

- If N > 50, $\sigma_{error} = \pm\sqrt{N_{SEE}}$
- If N < 50 the upper limit instead of the SEE number was used from Table 12, and the error is retrieved making the difference between the upper and lower cross section, assessed with the same table.

Whereas for N > 50 the σ_{error} can be positive or negative around the cross section value, for N < 50 the relative error can be only negative. Note that in Table 15 the associated flux to the ESA Monitor is retrieved averaging the fluxes from the 5 activation foils, whereas for what concern the Cypress memory the flux is that measured on the single foil placed to the center because the area of the latter is smaller compared with that of the ESA Monitor.

Memory	Setup	Test time [s]	Flux [n/cm2/s]	Fluence [n/cm2]	SEU	σ [cm2/bit]	% σ error
ESA Monitor 1330	no lid	180	1.28E+08	2.47E+10	1392	4.51E-15	± 2.68
Cypress 1437	center	1205	1.37E+08	1.65E+11	618	4.46E-16	± 4.02
Cypress 1443	center	1200	1.37E+08	1.64E+11	523	3.79E-16	± 4.37
Cypress 1443	center	1200	1.37E+08	1.64E+11	521	3.78E-16	± 4.38

Cypress 1443	center, B4C	300	1.37E+08	4.11E+10	3	2.55E-17	- 93.18

Table 15 - SEU tested SRAM memories at ILL, B4C means that 5 mm of boron carbide was covering the memory.

Memory	V	Test time [s]	Flux [n/cm2/s]	Fluence [n/cm2]	SEL	σ [cm2/chip]	% σ error
Brilliance x8	5.5V	1200	1.37E+08	1.64E+11	0	<2.81E-12	-

Table 16 - SEL tested SRAM memory at ILL.

6 Summary and conclusions

The LPSC and ILL facilities were cross-calibrated by means of the ESA SEU Reference monitor and with the objective of evaluating the facilities for possible qualification of components in the Radiation to Electronics (R2E) project context:

In LPSC, the relative flux values as a function of the distance to the target closely followed the expected r^{-2} dependence. The absolute cross section value for the 1104 date code was 9% larger than that retrieved at the PTB facility, and therefore mutually compatible when considering the associated fluence uncertainties.

As to what concerns ILL, the absolute cross section value was compatible with previous thermal neutron cross section measurements when considering possible sensitivity changes related to the use of different date codes, however, the beam measured by the ESA Monitor could not be considered homogeneous over an area typically representative of a component's sensitive surface (20 x 20 mm^2) whereas, from the facility calibration, it is homogeneous within 87% of the maximum intensity. The mismatch needs to be further investigated.

Moreover, whereas the SEU cross sections measured at 14 MeV were compatible with those obtained using higher energy protons (i.e. 200 MeV at PSI), the SEL values were significantly lower. As will be detailed in subsequent studies, this is compatible with the different sensitive volumes and LET responses associated to the individual SEE phenomena.

7 Acknowledgement

The authors would like to thank Maud Baylac and Francesca Villa from LPSC and Jerome Beaucour and Jaime Segura from ILL for the collaboration that enabled the use of the experimental beams, as well as for the support in the preparation, development and analysis of the test.
This work on D50 at the ILL and Genepi2 at LPSC (CNRS/UGA) has been performed within the "Characterisation Program" of the IRT nanoelec, co-funded by the French government in the frame of the so called "Programme d'Investissements d'Avenir" under the reference ANR-10-AIRT-05.

Bibliography

1] K. Roed, M. Brugger, D. Kramer, P. Peronnard, C. Pignard, G. Spiezia and A. Thorthon, "Method for Measuring Mixed Field Radiation Levels Relevant for SEEs at the LHC," *IEEE TRANSACTIONS ON NUCLEAR SCIENCE,* vol. 59, no. 4, pp. 1040-1047, 2012.

J. Beaucour, J. Segura-Ruiz, B. Giroud, E. Capria, E. Mitchell, C. Curfs, J. Royer,
2] M. Baylac, F. Villa and S. Rey, "Grenoble Large Scale Facilities for advanced characterisation of microelectronics devices," in *Radiation and Its Effects on Components and Systems (RADECS), 2015 15th European Conference on, DOI: 10.1109/RADECS.2015.7365616*, 2015.

D. Kramer, M. Brugger, V. Klupak, C. Pignard, K. Roed, G. Spiezia, L. Viererbl
3] and T. Wijnands, "LHC RadMon SRAM Detectors Used at Different Voltages to Determine the Thermal Neutron to High Energy Hadron Fluence Ratio," *IEEE TRANSACTIONS ON NUCLEAR SCIENCE,* vol. 58, no. 3, pp. 1117-1122, 2011.

[Online]. Available: http://avs.scitation.org/doi/10.1116/1.4907400.
4]

ILL - Institut Laue Langevin, "Rapport transparence et sécurité nucléaire – Institut
5] Laue Langevin," Grenoble, 2015.

F. Villa, M. Baylac, A. Billebaud, P. Boge, T. Cabanel, E. Labussière, O. Méplan
6] and S. Rey, "Multipurpose applications of the accelerator-based neutron source GENEPI2 (DOI 10.1393/ncc/i2015-15182-2)," *IL NUOVO CIMENTO,* vol. 38, no. C, p. 182, 2015.

R. Velazco, J. Clemente, G. Hubert, W. Mansour, C. Palomar, F. Franco, M.
7] Baylac, S. Rey, O. Rosetto and F. Villa, "Evidence of the Robustness of a COTS Soft-Error Free SRAM to Neutron Radiation," *IEEE TRANSACTIONS ON NUCLEAR SCIENCE,* vol. 61, no. 6, pp. 3103-3108, 2014.

D. Lambert, J. Baggio, G. Hubert, P. Paillet, S. Girard, V. Ferlet-Cavrois, O.
8] Flament, F. Saigne', J. Boch, B. Sagnes, N. Buard and T. Carrière, "Analysis of Quasi-Monoenergetic Neutron and Proton SEU Cross Sections for Terrestrial Applications," *IEEE TRANSACTIONS ON NUCLEAR SCIENCE,* vol. 53, no. 4, pp. 1890-1896, 2006.

B. Sierawski, K. Warren, R. Reed, R. Weller, M. Mendenhall and R. Schrimpf,
9] "Contribution of Low-Energy (<10 MeV) Neutrons to Upset Rate in a 65 nm SRAM," in *2010 IEEE International Reliability Physics Symposium, DOI: 10.1109/IRPS.2010.5488796*, 2010.

J. Autran, S. Serre, S. Semikh, D. Munteanu, G. Gasiot and P. Roche, "Soft-Error
10] Rate Induced by Thermal and Low Energy Neutrons in 40 nm SRAMs," *IEEE TRANSACTIONS ON NUCLEAR SCIENCE,* vol. 59, no. 6, pp. 2658-2665, 2012.

F. Villa, M. Baylac, S. Rey, O. Rossetto, W. Mansour, P. Ramos, R. Velazco and
11] G. Hubert, "Accelerator-based neutron irradiation of integrated circuits at GENEPI2 (France)," in *Radiation Effects Data Workshop (REDW), 2014 IEEE, DOI: 10.1109/REDW.2014.7004511*, 2014.

T. Lamy, J. Curdy, P. Sole, P. Sortais, T. Thuillier, J. Vieux-Rochaz and D. Voulot,

12] "Micro-PHOENIX: Intense deuton beams production for SPIRAL II," *Review of Scientific Instruments,* vol. 75, pp. 1485-1487, 2004.

13] "Low Activity Laboratory (LBA)," [Online]. Available: http://lpsc.in2p3.fr/index.php/en/plateformes-technologiques/lang-fr-lba-lang-lang-en-lba-lang.

14] G. Ban, J. Fontbonne, F. Lecolley, J. Lecolley, J. Lecouey, N. Marie, J. Steckmeyer, A. Billebaud, R. Brissot, C. Le Brun and E. Liatard, "A telescope for monitoring fast neutron sources," *Nuclear Instruments and Methods in Physics Research A,* vol. 577, p. 696–701, 2007.

15] "Atomic Weapon Establishment (AWE, UK), ASP," [Online]. Available: http://www.awe.co.uk/.

16] E. Blackmore, P. Dodd and M. Shaneyfelt, "Improved Capabilities for Proton and Neutron Irradiations at TRIUMF," in *Radiation Effects Data Workshop, 2003. IEEE, DOI:10.1109/REDW.2003.1281368*, 2003.

17] "KVI," [Online]. Available: http://www.rug.nl/kvi-cart.

18] R. Cubitt and J. Stahn, "Neutron reflectometry by refractive encoding," *THE EUROPEAN PHYSICAL JOURNAL PLUS,* 2011.

19] R. G. Alia, "Radiation Fields in High Energy Accelerators and their impact on Single Event Effects," in *Ph.D dissertation*, 2014.

20] R. Harboe-Sorensen, C. Poivey, F.-X. Guerre, A. Roseng, F. Lochon, G. Berger, W. Hajdas, A. Virtanen, H. Kettunen, and S. Duzellier, "From the Reference SEU Monitor to the Technology Demonstration Module On-Board PROBA-II," *IEEE TRANSACTIONS ON NUCLEAR SCIENCE,* vol. 55, 2008.

21] G. M. Swift, "SEE Testing Lessons from Dickens, Scouting, and Oz," Jet Propulsion Laboratory, California Institute of Technology.

22] K. Roed, M. Brugger, C. Pignard, "PTB Irradiation tests of the LHC Radiation Monitor (RadMon)," *ATS/Note/2011/012 TECH,* 2016.

23] F. Wrobel, J.-M. Palau, M.-C. Calvet, and P. Iacconi, "Contribution of SiO2 in Neutron-Induced SEU in SRAMs," *IEEE Transactions on Nuclear Science, Vol. 50, No.6* , December 2003.